Available online at www.sciencedirect.com
ScienceDirect
Comput. Methods Appl. Mech. Engrg. 305 (2016) 292–315
Computer methods in applied mechanics and engineering
www.elsevier.com/locate/cma

Formulation and numerical analysis of a fully-coupled dynamically deforming electromagnetic wire

Alejandro Francisco Queiruga*, Tarek I. Zohdi

Department of Mechanical Engineering, 6195 Etcheverry Hall, University of California, Berkeley, CA, 94720-1740, USA

Received 23 September 2015; received in revised form 1 January 2016; accepted 25 February 2016
Available online 16 March 2016

Abstract

An electromagnetic beam model is developed for the simulation of actuated electronic textiles. The beam is solved using a nonlinear director-based kinematic description with additional temperature and electric potential fields along its length. The three fields are fully coupled by mutual dependences on the deformation, Lorenz force, back electromotive force, temperature dependent constitutive responses, and the Seebeck effect. Instead of solving Maxwell's equations in full detail, a quasistatic approximation is used to solve the electric potential in the presence of a moving material medium. The current-carrying beam approximation is used to further simplify the solution space for the potential. While this formulation alleviates the spatial and temporal discretization restrictions, the coupled problem is an index-1 semi-explicit Differential Algebraic Equation requiring special treatment. The time dependent problem is solved using different Runge–Kutta methods. Diagonally implicit Runge–Kutta methods and explicit Runge–Kutta methods using implicit solution of the electric potential problem are explored. The finite element model is implemented using the open source package FEniCS, which is able to automatically generate the linearizations of the multiphysics equations required for the implicit solutions. A model problem is constructed with which to test and analyze the physical formulation and numerical solution techniques. The time stepping methods are verified using the convergence orders of the higher-order Runge–Kutta methods. Runtime comparisons show that the explicit methods are generally more computationally efficient than the implicit schemes used for this problem. For the implicit schemes, a staggered solution is significantly faster than a monolithic solution at most time step sizes. However, at very large time steps, such as those that would be used for dynamic relaxation, the monolithic solution can be more efficient than the staggered solution.

Keywords: Director-based beam model; Electromechanical modeling; Finite element method; Differential algebraic equation; Runge–Kutta methods

1. Introduction

The coupling of electromagnetic fields with moving and deforming structures is challenging to treat efficiently in a computational framework. This work presents a physical formulation and discusses numerical solution techniques

* Corresponding author.
E-mail address: afq@berkeley.edu (A.F. Queiruga).

http://dx.doi.org/10.1016/j.cma.2016.02.035

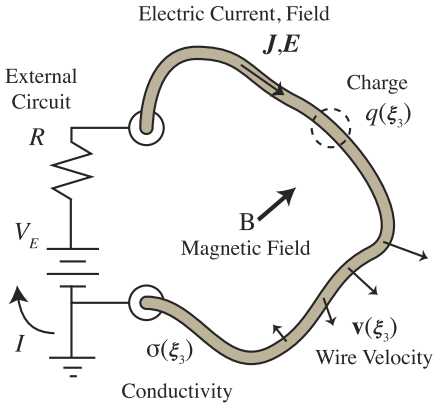

Fig. 1. A wire moving through a magnetic field.

for a slender yarn- or wire-like conductor moving and deforming through an applied magnetic field. The canonical setup studied is a single yarn clamped on both ends and connected to a simple resistor and voltage source circuit, diagrammed in Fig. 1. Such bodies can be found in MEMS devices [1,2] and electronic textiles [3,4]. The authors' greater interests include incorporation of the presented model into a simulation of electromagnetically actuated textiles, such as that seen in Haines [3] using electrothermal and thermomechanical effects.

The are two particular issues when coupling electromagnetism to structural problems that will be considered: (1) the spatial and temporal timescales associated with the electromagnetic fields yield very stiff numerical behavior, and (2) electromagnetic fields need to be solved in the interstitial and surrounding media and/or vacuum to the structure. A number of different formulations and numerical techniques have been used to solve coupled problems in electromagnetism. Often, Maxwell's equations are solved by discretizing the electric field **E** and flux density **B** directly and marching in time. Popular examples are the finite difference time domain method, introduced in Yee, 1966 [5], and specially designed vector-based finite elements such as the Nédélec elements introduced in 1980 [6]. Solving Maxwell's equations in time requires timesteps on the order of 10^{-14} s and similarly scaled spatial grids to discretize individual electromagnetic waves [7]. A finite element model solving **E** and **B** directly couples to the large deformation of a magnetoelastic membrane directly in Barham, 2010, using split implicit integration of the electromagnetic and mechanical fields [8]. The use of the electromagnetic potentials – e.g. the electric voltage potential V and magnetic vector potential **A** or other Gauge transforms on these – as primary solution variables is also possible. These formulations have the advantage of not requiring special elements to enforce divergence and curl conditions, so that nodal element basis functions can be used. For example, the finite element method is applied to solve the magnetic vector potential coupled to a saturable permeable material subject to deformations in Ren, 1995 [9] and Besbes, 1996 [10]. A discontinuous Galerkin enhanced immersed boundary finite element method for solving the electric scalar potential with material discontinuities is presented in Brandstetter, 2014 [11] that is used for problems in structure-interaction in Brandstetter, 2015 [12].

In this work, a novel formulation and discretization is used to avoid these issues. An electric potential formulation is developed that includes the theoretical treatment of motion and deformation of a conductor in a strong magnetic field. The geometry of the beam is used to further remove the need to solve the electromagnetic fields in the space around the material, allowing the same discretization to be used for the electric potential as is used for the mechanical and thermal fields. The stiff behavior of the potential and electric charge is used to develop a quasistatic approximation.

While this approach alleviates the temporal and spatial resolution restrictions on solving the electromagnetic fields, it introduces the additional complication of having to solve a Differential Algebraic Equation (DAE) to march the solution in time. These problems have the general form

$$0 = f\,(t, y, \dot{y}) \tag{1}$$

where t is time and y is the solution sought with time derivative $\dot{y}$. The problem reduces to an Ordinary Differential Equation (ODE) when f can be solved for $\dot{y}$ allowing the problem to be written as $\dot{y} = f\,(t, y)$. The index of a DAE, (or differentiability index, specifically) refers to how many time-derivatives must be taken of the system to produce an equivalent ODE. This value is used as a measure of the difficulty of solving the DAE [13]. Index reduction is one

methodology used to solve DAEs, wherein the equations are transformed by successive differentiation to produce an equivalent ODE. The methodology can be applied automatically using, e.g., the Pantelides algorithm [14]. However, index reduction typically results in issues such as error-drifting in constraints and is not necessary for index-1 DAEs [13]. Without resorting to index reduction, the solution of a DAE requires some type of implicit scheme. Methods designed for stiff problems are typically used. The Radau family of implicit Runge–Kutta methods is widely used, particularly Radau-IIa [15,16], which exhibits L-stability (i.e., the methods are designed to dampen stiff modes).

For the problem explored in this paper, the Voltage variable V produces an index-1 semi-explicit DAE with the structure

$$\dot{y} = f(t, y, V) \tag{2}$$

$$0 = g(t, y, V) \tag{3}$$

where g can be solved for V given a t and y. Taking advantage of this structure, this work explores the application of time stepping methods that are less-robust than those discussed above to determine an efficient solution method for the problem of discussion. The fully implicit methods, described above, such as the Radau family, require solving multiple stages simultaneously. This work applies Diagonally Implicit Runge–Kutta (DIRK) methods that only require solving a single stage at a time, resulting in smaller linear problems to solve and store. Through numerical experimentation, it is observed that the DAE does not require a time-stepping method that can handle stiffness. Thus, both L-stable and not L-stable implicit methods will be applied and compared. For further experimentation, the nonlinear stages of the implicit methods are solved in two ways: (1) using a monolithic solution of all fields simultaneously as a single DAE, and (2) decoupling the fields into three separate ordinary and implicit equations and solving each stage iteratively in a staggered fashion. Because the applied method does not need to handle stiffness, explicit Runge–Kutta methods can also be applied by using a solution method that solves the implicit Eq. (3) at every stage calculation of Eq. (2). Three different types of time-steppers and solution methods are applied to the DAE: explicit Runge–Kutta methods, diagonally implicit Runge–Kutta methods with monolithic stage solution, and diagonally implicit Runge–Kutta methods with staggered stage solution. Each of these methods is applied to schemes with different convergence orders.

The finite element method is used for the spatial discretization of the problem, using the open source FEniCS package for its implementation [17]. FEniCS employs a Domain Specific Language (DSL) to represent user-input variational forms that are then compiled into low-level C++ finite element routines, simplifying the implementation of the complicated system of equations formulated. The DSL system can perform differentiation to automatically obtain the tangent matrices to the finite element forms that are used in the solution of the nonlinear DAE [18]. A methodology for using FEniCS to automatically produce the finite element code needed to solve DAE by organization of the unknown fields into mixed function spaces is described.

The first half of the paper describes through the formulation of the dynamic current-carrying flexible wire. In Section 2, the Partial Differential Equations (PDEs) used as the basis of the model are developed from the theory of coupled continuum electromagnetism and mechanics. Next, the PDEs are further simplified in Section 3 using the assumed forms for the fields based on the geometry of the beam. The second half of the paper describes and analyzes the numerical solution methods. The variational form and the beam-specific integration methods used in the finite element discretization of the spatial equations are given in Section 4. Solution methods using explicit and implicit Runge–Kutta methods are described Section 5. Details of the implementation of the program, as well as external libraries used, are given in Section 6. The time integration methods are studied and compared on a model problem in Section 7. Finally, concluding remarks are given in Section 8.

2. Formulation

In this section, the PDE description of the problem is developed. The formulation of the system follows closely from Kovetz [19] and Steigmann [20]. For the reader's reference, the notation used in this section and the rest of the manuscript is summarized in Table 1. First, the special treatment of electromagnetic quantities with respect to deforming material frames is introduced in Section 2.1. The complete statements of the mechanical balance laws and Maxwell's equations for moving media in Section 2.2 are expressed. The constitutive models that will be used for the material media studied in this work are introduced in Section 2.3. With these, and additional assumptions about the electromagnetic fields in the problem, Maxwell's equations are reduced into a quasistatic electrostatic potential equation in Section 2.3.

Table 1
Nomenclature of operators and mechanical quantities.

Mechanics:	
$\mathbf{e}_i$	Coordinate orthonormal basis in spatial configuration
$\mathbf{E}_i$	Coordinate basis in a reference configuration
$\mathbf{x}$, $\mathbf{X}$, $\boldsymbol{\xi}$	Material position in current, reference, and ideal configurations, respectively.
$\mathbf{v}$	Material velocity
$\mathbf{F}$,	Deformation gradient with respect to reference configuration, $\frac{\partial \mathbf{x}}{\partial \mathbf{X}}$
T	Temperature
ρ	Mass density
$\mathbf{T}$	Cauchy stress tensor (current configuration)
u	Total material internal energy
$\mathbf{q}$	Heat flux vector
Electromagnetism:	
$\mathbf{E}$, $\mathbf{H}$	Electric field and magnetizing field (laboratory frame)
$\mathbf{B}$, $\mathbf{D}$	Magnetic flux density and electric displacement field (Galilean invariant)
V	Electric voltage potential (laboratory frame)
q	Free charge density (Galilean invariant)
$\mathbf{J}$	Current density (laboratory frame)
$\boldsymbol{\mathcal{J}}$	Conduction current density (material rest frame)
$\boldsymbol{\mathcal{E}}$	Electromotive intensity (material rest frame)
$\bar{r}$, $\bar{J}$	Mixed boundary condition coefficients
Constitutive properties:	
λ, μ, α_λ, α_μ	Lamé parameters and respective temperature coefficients
ϵ_0, μ_0	Permittivity and permeability of free space
$\mathbf{k}$	Thermal conductivity
$\boldsymbol{\chi}$	Relative electric susceptibility
$\boldsymbol{\sigma}$	Electric conductivity
S	Seebeck coefficient
Beam formulation:	
$\mathbf{r}$, $\mathbf{g}_1$, $\mathbf{g}_2$	Centroid position and director fields

2.1. Mechanical and electromagnetic coordinate frames

For a fully nonlinear body interacting with electromagnetic fields, there are a few different coordinate systems that need to be used. The kinematic frames that correspond to classical continuum mechanics are illustrated in Fig. 2. The coordinate system $\boldsymbol{\xi}$ is defined to provide a convenient description of the geometry of the body—in this case a long and thin beam. The reference (or, natural, or unstrained) configuration, $\mathbf{X}$, may differ from this ideal configuration; i.e., a beam may be naturally bent, but it is still easier to describe its deformation using the curvilinear system $\boldsymbol{\xi}$. The quantity $\mathbf{F} = \frac{\partial \mathbf{x}}{\partial \mathbf{X}}$ denotes the deformation gradient from the reference configuration to the current configuration of the body.

The treatment of electromagnetism requires one additional distinction to be made in the current configuration: the stationary laboratory frame and the rest frame of the material. No deformation field between the two is needed, but the material velocity $\mathbf{v}$ introduces new electromagnetic quantities. The displacement field, polarization density, and magnetic flux density are invariant, i.e. $\mathbf{D}^+ = \mathbf{D}$, $\mathbf{P}^+ = \mathbf{P}$, and $\mathbf{B}^+ = \mathbf{B}$. The current, $\mathbf{J}$, electric field, $\mathbf{E}$, magnetizing field, $\mathbf{H}$, and magnetization, $\mathbf{M}$, are not invariant, however, and in their place the conduction current density, $\boldsymbol{\mathcal{J}}$, the electromotive intensity, $\boldsymbol{\mathcal{E}}$, magnetomotive intensity, $\boldsymbol{\mathcal{H}}$, and Lorentz magnetization, $\boldsymbol{\mathcal{M}}$, are used:

$$\boldsymbol{\mathcal{J}} = \mathbf{J} - q\mathbf{v} \tag{4}$$

$$\boldsymbol{\mathcal{E}} = \mathbf{E} + \mathbf{v} \times \mathbf{B} \tag{5}$$

$$\boldsymbol{\mathcal{H}} = \mathbf{H} - \mathbf{v} \times \mathbf{D} \tag{6}$$

$$\boldsymbol{\mathcal{M}} = \mathbf{M} - \mathbf{v} \times \mathbf{D}. \tag{7}$$

In these equations, $\mathbf{v}$ is the material velocity, so that these quantities describe the fields in the material rest frame with respect to any Galilean frame (the material velocity $\mathbf{v}$ also transforms with respect to a new frame).

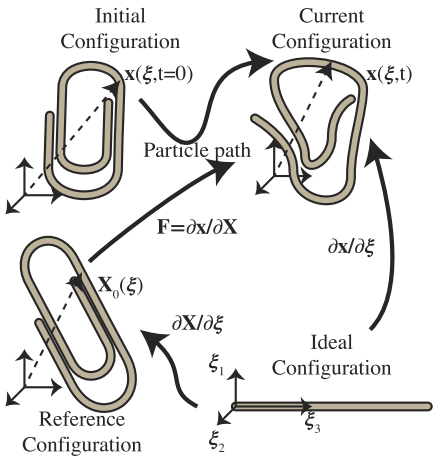

Fig. 2. Configurations for describing finite deformation problems. In this problem, the reference configuration is straight, so that $\boldsymbol{\xi} = \mathbf{X}$.

The Aether relations, describing the polarization and magnetization of free space, only hold in the stationary laboratory frame, but material constitutive responses require the Galilean invariant electric fields observed in the material's rest frame. The total displacement and magnetizing fields in the presence of the material are thus given by

$$\mathbf{D} = \epsilon_0 \mathbf{E} + \mathbf{P} \tag{8}$$

$$\boldsymbol{\mathcal{H}} = \mu_0^{-1} \mathbf{B} - \mathbf{v} \times \epsilon_0 \mathbf{E} - \boldsymbol{\mathcal{M}} \tag{9}$$

where ϵ_0 and μ_0 are the permittivity and permeability of free space. Since material responses must be specified in the material rest frame, this requires carefully distinguishing between both laboratory frame and material frame quantities.

2.2. Problem statements

The invariant forms of Maxwell's equations are

$$\nabla_x \cdot \mathbf{B} = 0 \qquad \nabla_x \times \boldsymbol{\mathcal{E}} = -\overset{*}{\mathbf{B}} \tag{10}$$

$$\nabla_x \cdot \mathbf{D} = q \qquad \nabla_x \times \boldsymbol{\mathcal{H}} = -\overset{*}{\mathbf{D}} + \boldsymbol{\mathcal{J}} \tag{11}$$

where $\overset{*}{\mathbf{X}}$ denotes the flux derivative, $\overset{*}{\mathbf{X}} = \frac{\partial \mathbf{X}}{\partial t} + (\nabla_x \cdot \mathbf{X})\,\mathbf{v} - \nabla_x \times (\mathbf{v} \times \mathbf{X})$. Additionally, charge conservation can be recovered from these equations,

$$-\frac{\partial q}{\partial t} = \nabla_x \cdot \mathbf{J} = \nabla_x \cdot (\boldsymbol{\mathcal{J}} + q\mathbf{v})\,. \tag{12}$$

The quantities q and $\boldsymbol{\mathcal{J}}$ are the free charge density and conduction current density that are "dragged" by the material.

The balance of energy and balance of linear momentum for the material medium are

$$\rho \left(\dot{u} - \frac{\partial u}{\mathbf{v}} \cdot \dot{\mathbf{v}} - \frac{\partial u}{\mathbf{F}} : \dot{\mathbf{F}} \right) = -\nabla_x \cdot \mathbf{q} + \rho h + \boldsymbol{\mathcal{J}} \cdot \boldsymbol{\mathcal{E}} \tag{13}$$

$$\rho \dot{\mathbf{v}} = \nabla_x \cdot \mathbf{T} + \rho \mathbf{b} + q\boldsymbol{\mathcal{E}} + \boldsymbol{\mathcal{J}} \times \mathbf{B}. \tag{14}$$

The terms ρu and $\rho \mathbf{v}$, and $\mathbf{T}$ are the internal energy, momentum, and Cauchy stress tensor of the material body itself. In the above equations, h and $\mathbf{b}$ are heat sources and body forces that are not electromagnetic in nature. The balance of energy equation has the additional terms $-\mathbf{P} \cdot \dot{\boldsymbol{\mathcal{E}}} - \boldsymbol{\mathcal{M}} \cdot \mathbf{B}$ on the right hand side, and the balance of linear momentum equation has the additional terms $+[\nabla_x \mathbf{P}]\,\boldsymbol{\mathcal{E}} + \overset{*}{\mathbf{P}} \times \mathbf{B} + [\nabla_x \boldsymbol{\mathcal{M}}]\,\mathbf{B} + \boldsymbol{\mathcal{M}} \times (\nabla_x \times \mathbf{B})$. These terms are present in the complete formulation and denote power and force terms on the body from the polarization and magnetization, but since polarizations and magnetizations will not be considered, these terms are left out for compactness.

The stored energy and momentum in the electromagnetic field are not present in Eqs. (13) and (14) This is a result of manipulation of Kovetz's original statements into a body-force and heat-source style equation on the material. Indeed, the balances stored energy and momentum of the electromagnetic fields are automatically satisfied by Maxwell's equations (Eqs. (10) and (11)), and do not need to be considered in their solution. The energy and momentum of the fields can be post-processed out of a solution to these PDEs if desired.

2.3. Constitutive responses

The following quantities remain that require constitutive responses:

$$u, \mathbf{q}, \boldsymbol{\mathcal{J}}, \mathbf{T}, \mathbf{P}, \boldsymbol{\mathcal{M}}. \tag{15}$$

The internal stored energy has the following relations:

$$\mathbf{T} = \frac{\partial u}{\partial \mathbf{F}}\mathbf{F}^T, \qquad \mathbf{P} = -\rho\frac{\partial u}{\partial \boldsymbol{\mathcal{E}}}, \qquad \boldsymbol{\mathcal{M}} = -\rho\frac{\partial u}{\partial \mathbf{B}}. \tag{16}$$

Thus, only u, $\mathbf{q}$, and $\boldsymbol{\mathcal{J}}$ need to be specified, (though the effort to specifying u does increase).

The variable u denotes the internal stored energy of the material, not including that contained in the $\mathbf{E}$ and $\mathbf{B}$ fields themselves. For a general class of solids, it is a function of deformation gradient, temperature, and the electromagnetic fields, $u = \hat{u}(\mathbf{F}, T, \boldsymbol{\mathcal{E}}, \mathbf{B})$. Explicit dependences for electromechanical effects, such as piezoelectricity, will not be considered, though the theoretical and computational formulation makes it possible to consider them. A general elastic dielectric will have a constitutive response of $u(T, \mathbf{F}, \boldsymbol{\mathcal{E}}) = u_{heat}(T) + u_{strain}\left(T, \mathbf{F}^T\mathbf{F}\right) + u_{polar}(\boldsymbol{\mathcal{E}})$. For a linear dielectric, the polarization is $\mathbf{P}' = \epsilon_0\boldsymbol{\chi}\boldsymbol{\mathcal{E}}$ where $\boldsymbol{\chi}$ is the relative susceptibility of the material and ϵ_0 is the free space permittivity. $u_{polar} = -\frac{1}{2}\boldsymbol{\mathcal{E}}\cdot\epsilon_0\boldsymbol{\chi}\boldsymbol{\mathcal{E}}$. The term $\frac{\partial u}{\partial \boldsymbol{\mathcal{E}}}\cdot\dot{\boldsymbol{\mathcal{E}}}$ would appear in Eq. (13) and would greatly complicating the solution process, so polarization is not included in the implementation. The constitutive response of the material used is a temperature dependent Neohookean hyperelastic stress with a linear heat capacity:

$$u = \underbrace{c_v(T - T_0)}_{u_{heat}} + \underbrace{\frac{\mu(T)}{2}(\mathrm{tr}\mathbf{C} - 3) - \mu(T)\log J + \frac{\lambda(T)}{2}\log^2 J}_{u_{strain}}, \tag{17}$$

where T_0 is a reference temperature. The Lamé parameters μ and λ can be calculated from Young's modulus E and Poisson ratio ν by $\mu = \frac{E}{2(1+\nu)}$ and $\lambda = \frac{E\nu}{(1+\nu)(1-2\nu)}$. A linear temperature dependence is used in the material parameters, $\mu(T) = \mu_0 + \alpha_\mu(T - T_0)$ and $\lambda(T) = \lambda_0 + \alpha_\lambda(T - T_0)$, where μ_0 and λ_0 are the reference-temperature values.

Fourier's law for heat flux is used, which relates the heat flux $\mathbf{q}$ to the temperature gradient by

$$\mathbf{q} = -\mathbf{k}\nabla_x T \tag{18}$$

where $\mathbf{k}$ is the thermal conductivity tensor. Only isotropic materials are considered, so the thermal conductivity $\mathbf{k}$ will be treated as a scalar.

Ohm's law for a conductor, $\boldsymbol{\mathcal{J}} = \boldsymbol{\sigma}\boldsymbol{\mathcal{E}}$, where $\boldsymbol{\sigma}$ is the electrical conductivity tensor, also holds in the material's rest frame (see [21] p572; [19] p86, 135). As with the thermal conductivity, only isotropic materials are considered, so it will be treated as a scalar. Additionally, the Seebeck effect will be considered, which induces an electromotive force in response to temperature gradients. The constitutive response for the material is

$$\boldsymbol{\mathcal{J}} = \boldsymbol{\sigma}(\boldsymbol{\mathcal{E}} - S\nabla_x T) \tag{19}$$

where S is the Seebeck coefficient that can be either positive or negative, depending on the material. The reader is directed to Kovetz [19] for a formal development of electromagnetic material constitutive responses.

The material laws are specified in the reference state of the material, and transform due to the deformation of the material as $\mathbf{k} = \frac{1}{J}\mathbf{F}\mathbf{k}_0\mathbf{F}^T$, $\boldsymbol{\sigma} = \frac{1}{J}\mathbf{F}\boldsymbol{\sigma}_0\mathbf{F}^T$, and $\boldsymbol{\chi} = \frac{1}{J}\mathbf{F}\boldsymbol{\chi}_0\mathbf{F}^T$. A material that is isotropic in its reference frame develops a texture due to its deformation. Thus, isotropy is the statement about the reference values $\boldsymbol{\sigma}_0 = \hat{\sigma}\mathbf{I}$, $\mathbf{k}_0 = \hat{k}\mathbf{I}$, and $\boldsymbol{\chi}_0 = \hat{\chi}\mathbf{I}$, where $\mathbf{I}$ is the identity matrix.

2.4. Electric potential approximation

The following assumptions are used to further simplify the electromagnetic problem state:

1. The magnetic B field is dominated by an externally applied field (such as a powerful electromagnet near the wire); the contribution by the current in the conductor is negligible, i.e. $B_{app} \gg B_{self}$. This assumption implies that the electromotive force introduced by the motion of the conductor through the external source is greater than the self-electromotive force due to the self-inductance of the conductor.[1]
2. The time behavior of the E field and charge is highly stiff on mechanical time scales, $\frac{\epsilon_0(1+\chi)}{\sigma} \to 0$.
3. The effect of the electric charge density inside of the conductor is negligible as the force magnitude from the electric current component of the Lorenz force is much greater than the electric charge component, $\mathcal{J} \times \mathbf{B} \gg q\boldsymbol{\mathcal{E}}$.

These assumptions are used to replace Maxwell's equations with a simpler PDE to solve. The electric potential is not invariant, but the invariant quantity $V' = V - \mathbf{v} \cdot \mathbf{A}$ is unwieldy for this formulation due to its dependence on the magnetic vector potential, $\mathbf{A}$. Let V be the *Lab Frame* electric potential so that the electric field $\mathbf{E}$ then satisfies $\mathbf{E} = -\nabla_x V$. Faraday's law, $\nabla \times \mathbf{E} = \frac{\partial \mathbf{B}}{\partial t}$ is trivially satisfied by this formulation, since the curl of the gradient is zero, and Gauss's law for magnetism, $\nabla \cdot \mathbf{B} = 0$ forms a constraint on the applied $\mathbf{B}$ that can be chosen. The derivation begins with Gauss's law $\nabla \cdot \mathbf{D} = q$ and charge conservation, $\frac{\partial q}{\partial t} + \nabla \cdot \mathbf{J} = 0$. In these two equations, there are two unknowns: the electric potential V and the charge q.

First, the constitutive responses are inserted into the law for charge conservation, $-\frac{\partial q}{\partial t} = \nabla_x \cdot (\boldsymbol{\sigma} (\boldsymbol{\mathcal{E}} - S\nabla_x T)) + \nabla_x \cdot q\mathbf{v}$, and into Gauss's law, $q = \nabla_x \cdot \epsilon_0 (\mathbf{E} + \boldsymbol{\chi}\boldsymbol{\mathcal{E}})$. (The susceptibility of the wire of question is zero, but is included in this discussion for future use.) The potential is plugged into both of these equations to obtain

$$\frac{\partial q}{\partial t} + \nabla_x \cdot q\mathbf{v} = \nabla_x \cdot \boldsymbol{\sigma} \nabla_x V - \nabla_x \cdot \boldsymbol{\sigma} (\mathbf{v} \times \mathbf{B} - S\nabla_x T) \tag{20}$$

$$q = -\nabla_x \cdot \epsilon_0 (\mathbf{I} + \boldsymbol{\chi}) \nabla_x V + \nabla_x \cdot \epsilon_0 \boldsymbol{\chi} \mathbf{v} \times \mathbf{B}. \tag{21}$$

Let $\frac{Dq}{Dt} = \frac{\partial q}{\partial t} + \nabla \cdot (q\mathbf{v})$. For the sake of a scaling argument, the conductivity is decomposed into a constant scaling factor and a fabric tensor by $\boldsymbol{\sigma} = \hat{\sigma}\mathbf{A}_\sigma$ where $\|\mathbf{A}_\sigma\| \approx 1$. After substituting Eq. (21) into Eq. (20), the following first-order ODE for the voltage is obtained (where D/Dt contains the additional convection term):

$$-\frac{\epsilon_0}{\hat{\sigma}} \frac{D}{Dt} (\nabla_x \cdot (\mathbf{I} + \boldsymbol{\chi}) \nabla_x V - \nabla_x \cdot (\boldsymbol{\chi} \mathbf{v} \times \mathbf{B})) = \nabla_x \cdot \mathbf{A}_\sigma \nabla_x V - \nabla \cdot_x \mathbf{A}_\sigma (\mathbf{v} \times \mathbf{B} - S\nabla_x T). \tag{22}$$

The permittivity of free space ϵ_0 is approximately equal to 8.85×10^{-12} $\frac{\mathrm{F}}{\mathrm{m}}$ and the conductivity σ of conductors is on the order of 10^6 $\frac{\mathrm{S}}{\mathrm{m}}$. The susceptibility χ of materials is close to zero or one. For most materials, the ratio $\frac{\epsilon_0(1+\chi)}{\hat{\sigma}}$ is extremely small and represents a very stiff time constant for the relaxation time of the free charges and electric potential. Taking the limit as $\frac{\epsilon_0}{\hat{\sigma}} \to 0$, the steady state result can be used as an approximation,

$$\nabla_x \cdot \boldsymbol{\sigma} \nabla_x V = \nabla_x \cdot \boldsymbol{\sigma} (\mathbf{v} \times \mathbf{B} - S\nabla_x T), \tag{23}$$

where the conductivity tensor $\boldsymbol{\sigma}$ is written again for clarity. This equation is a quasistatic potential approximation for a deforming material moving through a magnetic field with an induced electromotive force (the term $-S\nabla_x T$ can be exchanged by any other response). From the solution of the potential, the quasistatic value of the free charge q can be determined by Gauss's law.

The fact that there is a charge density present is contrary to experience with the analysis of stationary conductors. A standard conductor (no additional chemical potential) moving in a magnetic field will develop a charge density

[1] A corresponding circuit approximation would have the assumption $EMF_{applied} \gg \frac{d}{dt}\left(L_{self} I\right)$. To estimate L_{self}, consider the case where the wire is deformed into a semi-circle and the external circuit is also laid out in a semi circle of radius $r = \frac{L}{2} = 1$ mm. Then, the inductance is $L = \mu_0 r \left(\log\left(\frac{8r}{R}\right) - 2 + \frac{Y}{2}\right)$, Y is the skin correction factor. Following the Ansatz of uniformly distributed current ($Y = 1/2$) and using the wire dimensions, $L \approx 5.32 \times 10^{-9}$ F. Additionally, the current is of magnitude $I \approx 10^{-4}$ A in the problem. With a simulation duration of 2.5 ms and assuming a zero-to-maximum change (which is not the case since L and I are not initially zero), the term $\frac{d}{dt}\left(L_{self} I\right)$ can be capped by 10^{-9} V. With a 1 T applied field, $EMF_{applied} = \int vBdl \approx 1\ \frac{\mathrm{m}}{\mathrm{s}} \times 1\ \mathrm{T} \times 0.002\ \mathrm{m} = 0.002$ V, justifying the assumption.

according to $q = \epsilon_0 \nabla_x \cdot \mathbf{v} \times \mathbf{B}$. Note that another commonly analyzed state of the conductor rigidly translating through the medium will also not produce a charge density, only surface charges at opposite ends. A conductor rotating with constant angular velocity about an axis, e.g. $\mathbf{v} = \omega r \mathbf{e}_\theta$, will develop a constant charge density. If the magnetic field is along the axis, then $q = \epsilon_0 2\omega B$. For an example of such a system, consider the Faraday disc (i.e., a homopolar generator) (see Kovetz, p139, and Montgomery, 2003 [19,22]).

However, the post-processing step to calculate q is extra computational work. The magnitude of the force density $q\mathcal{E} = q\,(\mathbf{E} + \mathbf{v} \times \mathbf{B})$ is much smaller than the magnitude of the term $\mathcal{J} \times \mathbf{B}$ and is neglected.[2] Thus, the force density for the beam is only calculated by $\mathbf{f} \approx \mathcal{J} \times \mathbf{B}$.

2.5. Electric boundary conditions

Boundary conditions are desired that would yield a back electromotive force effect, as is observed in an electric motor, for example. Using two Dirichlet voltage boundary conditions has current-sourcing effects that are not intuitive. One side of the wire is set to ground to pin the constant mode in the PDE, and on the other side, a mixed boundary condition is used that couples the body to the external circuit illustrated in Fig. 1.

The total current leaving the body and entering the circuit is $I = \int_\Gamma \mathcal{J} \cdot \mathbf{n} d\Gamma$. Assuming $V\,(0) = 0$ V, the body has to match up with the circuit by the integral relation

$$V\,(L) = -R \int_\Gamma \mathcal{J}\,(L) \cdot \mathbf{n} d\Gamma + \Delta V_E, \tag{24}$$

where R is an external resistance and ΔV_E is an external voltage source. Assuming that there is an ideal electrical connection at the surface, with the area of the surface being A, the above relation can be phrased in terms of the current density as

$$\mathcal{J}\,(L) \cdot \mathbf{n} = \underbrace{-\frac{1}{RA}}_{\bar{r}} V\,(L) + \underbrace{\frac{\Delta V_E}{RA}}_{\bar{J}}, \tag{25}$$

thus giving a mixed boundary condition linearly relating the normal current density to the potential with coefficients $\bar{r}$ and $\bar{J}$. Coupling to more complicated circuits requires solving an additional Kirchhoff's law network system while solving the PDE.

2.6. Summary of field equations

In a standard approach to solving solid deformations, the partial differential equations are pushed back into the reference configuration. A subscript naught denotes a value evaluated in the material reference configuration. The three coupled partial differential equations derived can be summarized by

$$\rho_0 \ddot{\mathbf{x}} = \nabla_X \cdot \frac{\partial u}{\partial \mathbf{F}} + \frac{\rho_0}{\rho} \mathcal{J} \times \mathbf{B} + \rho_0 \mathbf{b} \tag{26}$$

$$\left(\rho_0 c_p + \frac{\partial u_{strain}}{\partial T}\right) \dot{T} = \nabla_X \cdot \mathbf{k}_0 \nabla_X T + \frac{\rho_0}{\rho} \mathcal{J} \cdot \mathcal{E} + \rho_0 h \tag{27}$$

$$0 = \nabla_X \cdot \boldsymbol{\sigma}_0 \nabla_X V - \nabla_X \cdot \boldsymbol{\sigma}_0 \left(\mathbf{F}^T \mathbf{v} \times \mathbf{B} - S_0 \nabla_X T\right) \tag{28}$$

where the material position was written, $\dot{\mathbf{x}} = \mathbf{v}$, and $\mathbf{b}$ and h are specific forces and heating terms that are not electromagnetic in nature. The three fields are fully coupled, illustrated in Fig. 3. No extra heating term is included,

[2] Consider a 1 mm long beam with a 0.1 mm cross sectional radius moving perpendicular to a magnetic field of 1 T with a velocity of 100 m/s and 0 m/s at either end. A back-of-the-envelop calculation shows that the force density magnitude $\left(\epsilon_0 \frac{\Delta v}{L} B\right)(vB) = 8.85 \times 10^{-12}$ F/m $\times$ 100 m/s $\times$ 1 T/10^{-3} m is approximately 8.85×10^{-5} N/m^3. For comparison, if the beam were carrying 10^{-4} A of current, the force density, $IB/A = 1A \times 1\,\mathrm{T}/\left(\pi\,(0.1\text{ mm})^2\right)$, is approximately 3.1×10^3 N/m^3.

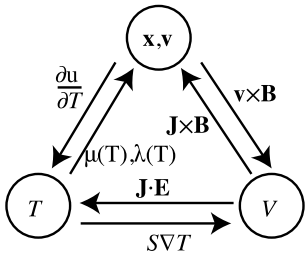

Fig. 3. Coupling diagram of fields.

$h = 0$, and, for the sake of numerical stability, a dampening body force of $\mathbf{b} = -\gamma \mathbf{v}$ is used. The conduction current density can be determined from the potential field by

$$\mathcal{J} = \frac{1}{J}\mathbf{F}\sigma_0\mathbf{F}^T\left(\underbrace{-\mathbf{F}^{-T}\nabla_X V + \mathbf{v}\times\mathbf{B}}_{=\boldsymbol{\mathcal{E}}} + \underbrace{S\mathbf{F}^{-T}\nabla_X T}_{S\nabla_x T}\right). \tag{29}$$

The push-back into the ideal configuration is identical, with all reference configuration values, subscript X and 0, replaced by their values in the ideal configuration, subscript ξ. The reference configuration does not differ from the ideal configuration in the model problem studied.

Remark: fully-coupling the problem

The Seebeck effect was included in the problem for the sake of the numerical study. A missing arrow in Fig. 3 would correspond to a zero-block in the tangent matrix seen later in Eq. (91). Out of concerns that a zero-block in the matrix might bias one solution method over another, the Seebeck effect was added as the simplest way to fill out the matrix. That is, the effect was added to make the problem "harder" with respect to the solution algorithm.

3. Current-carrying beam

A kinematic director-based beam model is used, wherein in a one dimensional finite element basis is used along the axis and an ansatz is used along the cross section to construct the displacement field using two vector directors, as diagrammed in Fig. 4. E.g, see Rubin [23]. Thermal and electromagnetic fields are incorporated into the beam formulation with additional ansätze for the temperature and electric current that are constant along the cross section.

3.1. Director-based beam model

The ideal configuration of the beam has coordinates X_1, X_2 along the cross section and X_3 along the axis, with the curvilinear orthonormal basis vectors $\mathbf{E}_1$, $\mathbf{E}_2$, and $\mathbf{E}_3$, respectively. Let $\mathbf{r}(X_3)$ denote the position of the centroid of a given cross section of the wire, and $\mathbf{g}_1(X_3)$ and $\mathbf{g}_2(X_3)$ denote directors of the cross section in the directions X_1 and X_2. These fields are assembled into an assumed solution for the position field

$$\mathbf{x}(X_1, X_2, X_3, t) = \mathbf{r}(X_3, t) + X_1\mathbf{g}_1(X_3, t) + X_2\mathbf{g}_2(X_3, t). \tag{30}$$

The director fields are illustrated in Fig. 4. The coordinate system $\boldsymbol{\xi}$ was defined for convenient description of the geometry of the long and thin fiber to allow this simplified deformation description. The reference (or, natural, or unstrained) configuration, $\mathbf{X}$, may differ from this ideal configuration; i.e., a fiber may be naturally bent, but it is still easier to describe its deformation using the curvilinear system $\boldsymbol{\xi}$. The configurations are illustrated in Fig. 2.

The deformation gradient for this field can be calculated by $\mathbf{F} = \frac{\partial \mathbf{x}}{\partial \mathbf{X}} = \frac{\partial \mathbf{x}}{\partial \boldsymbol{\xi}}\frac{\partial \boldsymbol{\xi}}{\partial \mathbf{X}_0} = \frac{\partial \mathbf{x}}{\partial \boldsymbol{\xi}}\left(\frac{\partial \mathbf{X}_0}{\partial \boldsymbol{\xi}}\right)^{-1}$ where $\mathbf{X}_0$ is the mapping from the ideal configuration $\boldsymbol{\xi}$ to the reference configuration $\mathbf{X}$. The gradient with respect to the ideal configuration is calculated from the ansatz by

$$\frac{\partial \mathbf{x}}{\partial \mathbf{X}} = \left(\frac{\partial \mathbf{r}}{\partial X_3} + X_1\frac{\partial \mathbf{g}_1}{\partial X_3} + X_2\frac{\partial \mathbf{g}_2}{\partial X_3}\right)\otimes\mathbf{E}_3 + \mathbf{g}_1\otimes\mathbf{E}_1 + \mathbf{g}_2\otimes\mathbf{E}_2. \tag{31}$$

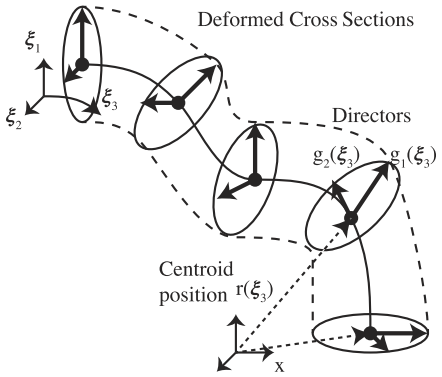

Fig. 4. Director based beam formulation.

If the unstrained configuration is assumed to be identical to the reference configuration, $\mathbf{X} = \boldsymbol{\xi}$, as is the case for an initially straight beam, then $\frac{\partial \mathbf{X}}{\partial \boldsymbol{\xi}} = \mathbf{I}$, and the deformation gradient is $\mathbf{F} = \frac{\partial \mathbf{x}}{\partial \boldsymbol{\xi}}$.

The unit normal to the cross section can be obtained by $\mathbf{n}_C\left(X_3\right) = \frac{\mathbf{g}_1 \times \mathbf{g}_2}{\|\mathbf{g}_1 \times \mathbf{g}_2\|_2}$. The cross section and centroid are not required to be perpendicular in the director-based theory. The unit vector along the centroid is defined in terms of the centroid position field by

$$\mathbf{e}_{axis}\left(X_3\right) = \frac{d\mathbf{r}/dX_3}{\|d\mathbf{r}/dX_3\|_2} \tag{32}$$

and is used to orient the electric current. In rotation-based beam models, this unit vector is obtained by applying the rotation matrix, $\mathbf{R}$, to the reference axis vector, $\mathbf{e}_{axis} = \mathbf{R}\mathbf{E}_3$.

3.2. Balance of energy

The beams are assumed to have a constant temperature across their cross section, so that the temperature is only a function of the axis coordinate,

$$T = T\left(X_3\right). \tag{33}$$

This representation can be plugged into the balance of energy laws directly. The gradient in the reference configuration is then only constructed from the derivative along the centroid direction,

$$\nabla_X T = \frac{dT}{dX_3}\mathbf{E}_3. \tag{34}$$

3.3. The restriction of electromagnetic problem to the beam

Without further assumptions, it would be necessary to mesh the space around the textile, even if it were a vacuum, and calculate the electromagnetic fields there as well. For this problem, it is assumed that the magnetic field is dominated by an externally applied source, such that the contributions by currents in the body are negligible. Only the electric field and current inside of the textile will be calculated during the simulation. The electric field outside of the material varies as a consequence but is not required for the deformation calculation.

The base assumption to the electromagnetic discretization is that the conduction current density is uniform across the cross section and oriented along the axis of the beam, such that

$$\boldsymbol{\mathcal{J}} = \mathcal{J}\left(X_3\right)\mathbf{e}_{axis}\left(X_3\right). \tag{35}$$

The notations used will now collide slightly with respect to the electric field and the ideal coordinate basis: $\mathbf{FE}_3 \parallel \mathbf{e}_{axis}$, $\mathbf{FE}_1$, and $\mathbf{FE}_2$ are the basis vectors of the reference coordinate system pushed into the current configuration. Because both the current and temperature gradient are assumed to be oriented along the axis of the fibril, the constitutive law of Eq. (19), $\boldsymbol{\mathcal{J}} = \sigma\left(\boldsymbol{\mathcal{E}} - S\nabla_x T\right)$, assuming isotropy, requires that electromotive intensity must also be oriented along the axis of the fibril, yielding $\boldsymbol{\mathcal{E}} \cdot \mathbf{FE}_1 = \boldsymbol{\mathcal{E}} \cdot \mathbf{FE}_2 = 0$. Using the above assumption the lab frame electric

field can be broken up into the curvilinear coordinates of the beam as $(\mathbf{E}+\mathbf{v}\times\mathbf{B})\cdot\mathbf{F}\mathbf{E}_1 = (\mathbf{E}+\mathbf{v}\times\mathbf{B})\cdot\mathbf{F}\mathbf{E}_2 = 0$. This yields the following restriction for the electric potential:

$$\mathbf{F}^T\nabla_x V\cdot\mathbf{E}_1 = \mathbf{F}^T(\mathbf{v}\times\mathbf{B})\cdot\mathbf{E}_1 \tag{36}$$

$$\mathbf{F}^T\nabla_x V\cdot\mathbf{E}_2 = \mathbf{F}^T(\mathbf{v}\times\mathbf{B})\cdot\mathbf{E}_2. \tag{37}$$

Even though the potential is being constructed in the lab frame, the condition that current must flow along the axis of the beam yields a trivial condition on the gradient of the voltage across the cross section. These components could be solved for by substituting in the ansatz for $\mathbf{v}$, but do not have any effect on the current and are thus uninteresting. Returning to the potential equation and breaking the divergence in the components along the ideal coordinates,

$$0 = \nabla_X\cdot\boldsymbol{\sigma}_0\nabla_X V - \nabla_X\cdot\boldsymbol{\sigma}_0 J\mathbf{F}^{-1}\mathbf{v}\times\mathbf{B} + \nabla_X\cdot\boldsymbol{\sigma}_0 S_0\nabla_X T. \tag{38}$$

Only the ξ_3 direction is not trivially satisfied by Eqs. (36) and (37), so the one-dimensional PDE that needs to be solved is

$$\frac{d}{dX_3}\boldsymbol{\sigma}_0\frac{dV}{dX_3} = \frac{d}{dX_3}\boldsymbol{\sigma}_0\left(\mathbf{v}\times\mathbf{B}\cdot\mathbf{F}\mathbf{E}_3 - S_0\frac{dT}{dX_3}\right). \tag{39}$$

Thus, for computation purposes, only voltage at the centroid of the beam needs to be solved, yielding an unknown field that is only a function of the axis coordinate,

$$V = V(X_3). \tag{40}$$

Since the only non-zero component of $\boldsymbol{\mathcal{E}}$ is along the axis coordinate, the conduction current density in the laboratory frame can be determined to depend on the laboratory frame voltage, the deformation gradient, the material velocity, and the temperature gradient by

$$\boldsymbol{\mathcal{J}} = \frac{1}{J}\mathbf{F}\boldsymbol{\sigma}_0\left(-\frac{\partial V}{\partial X_3} + \mathbf{F}^T\mathbf{v}\times\mathbf{B}\cdot\mathbf{E}_3 - S_0\frac{\partial T}{\partial X_3}\right)\mathbf{E}_3. \tag{41}$$

4. Variational form

4.1. Function spaces

The continuum problem has four unknown fields: $\mathbf{x}$, $\mathbf{v}$, T, V. In the kinematic beam model, the fields $\mathbf{x}$ and $\mathbf{v}$ have assumed forms that are not directly the functions being sought. The solutions that are sought are thus constructed from component functions of $\mathbf{r}$, $\mathbf{g}_1$ and $\mathbf{g}_2$. For the sake of clarity at the expense of compactness, the following naming convention for fields is adopted: prefix of δ denotes a test function, prefix of $\mathbf{v}$ denotes an element of the velocity field, and an overdot $\dot{a}$ denotes the time derivative, with an overline $\overline{abc}$ used to prevent ambiguity with multi-character symbols. There are eight unknown fields

$$\mathbf{r},\ \mathbf{g}_1,\ \mathbf{g}_2,\ \mathbf{v}\mathbf{r},\ \mathbf{v}\mathbf{g}_1,\ \mathbf{v}\mathbf{g}_2,\ T,\ V \tag{42}$$

with a total of twenty components. The following function spaces are defined for seeking the solutions for these fields:

$$\mathbf{r},\mathbf{v}\mathbf{r},\delta\mathbf{r} \in \mathcal{V}_r \tag{43}$$

$$\mathbf{g}_1,\mathbf{v}\mathbf{g}_1,\dot{\overline{\mathbf{v}\mathbf{g}}}_1,\mathbf{g}_2,\mathbf{v}\mathbf{g}_2,\dot{\overline{\mathbf{v}\mathbf{g}}}_1 \in \mathcal{V}_g \tag{44}$$

$$T,\dot{T},\delta T \in \mathcal{S}_T \tag{45}$$

$$V,\delta V \in S_V. \tag{46}$$

The test displacement and velocity fields constructed from test functions from the space of solutions of $\mathbf{r}$, $\mathbf{g}_1$, and $\mathbf{g}_2$, relating them to the test functions in the space of w by the relations

$$\delta\mathbf{x}(X_1,X_2,X_3) = \delta\mathbf{r}(X_3) + X_1\delta\mathbf{g}_1(X_3) + X_2\delta\mathbf{g}_2(X_3), \tag{47}$$

and, by stating that the position and velocities of the directors come form the same spaces, the test functions on the velocity are identical, $\delta\mathbf{v} = \delta\mathbf{x}$.

4.2. Integral statements

The integration over the domain is split between the cross section and the axis. The finite element approximation discretizes the solution along X_3, and the integral along $\int_0^L \mathrm{d}X_3$, where $X_3 \in [0, L]$, is handled by the finite element program. Integration over the cross section is evaluated by Gaussian quadrature, so that each Gauss point on the finite element discretization maps to multiple Gauss points on the cross section and its boundary. Let w^A, $\hat{X}_1^A$, $\hat{X}_2^A \in P(\Omega)$ denote the set of Gauss points and weights over the geometric quantity Ω.

Performing the integration of the PDEs over the domain of the beam, and applying the above described cross-section quadrature, yields the following finite element integrals. The subscript m denotes forms related to the mechanical fields, T denotes forms related to the temperature fields, and V denotes forms related to the Voltage fields. The masses for the mechanical and thermal forms are

$$\mathbb{M}_m(\delta v, \dot{v}) = \int_0^L \sum_{A\in P(C)} w^A \left(\delta\mathbf{vr} + \hat{X}_1^A \delta\mathbf{vg}_1 + \hat{X}_2^A \delta\mathbf{vg}_2\right) \cdot \rho \left(\dot{\overline{\mathbf{vr}}} + \hat{X}_1^A \dot{\overline{\mathbf{vg}_1}} + \hat{X}_2^A \dot{\overline{\mathbf{vg}_2}}\right) \mathrm{d}X_3 \tag{48}$$

$$\mathbb{M}_T\left(\delta T, \dot{T}\right) = \int_0^L \sum_{A\in P(C)} w^A \delta T \dot{T} \mathrm{d}X_3. \tag{49}$$

The internal force vector is formed by

$$\mathbb{F}_m(\delta v, v, x; T, V) = \int_0^L \left(\sum_{A\in P(C)} w^A \left(\delta\mathbf{x} \cdot \frac{\delta u}{\delta \mathbf{x}} + \delta\mathbf{x} \cdot \mathcal{J}\mathbf{e}_y \times \mathbf{B}\right) + \sum_{A\in P(\partial C)} w^A \delta\mathbf{x} \cdot \bar{\mathbf{p}} \right) \mathrm{d}X_3 \tag{50}$$

$$+ \left[\sum_{A\in P(C)} w^A \delta\mathbf{x} \cdot \bar{\mathbf{t}} \right]_0^L, \tag{51}$$

the thermal internal force by,

$$\mathbb{F}_T(\delta T, T; v, x, V) = \int_0^L \left(\sum_{A\in P(C)} w^A \frac{1}{\rho_0 c_p + \frac{\partial u_{strain}}{\partial T}} \left(\frac{d\delta T}{dX_3} k_0 \frac{dT}{dX_3} + \delta T \left(\sigma_0 \mathcal{J}^2\right)\right)\right) \mathrm{d}X_3 \tag{52}$$

$$+ \left[\sum_{A\in P(C)} w^A \delta T \cdot \bar{\mathbf{q}} \cdot \mathbf{n} \right]_0^L, \tag{53}$$

and the implicit voltage equation satisfies the variational integral

$$\mathbb{G}_V(\delta V, V; v, x, T) = \int_0^L \sum_{A\in P(C)} w^A \left(\frac{d\delta V}{dX_3} \boldsymbol{\sigma}_0 \frac{dV}{dX_3} + \frac{d\delta V}{dX_3} \mathbf{E}_3 \cdot \mathbf{F}^T \mathbf{v} \times \mathbf{B} \cdot \mathbf{E}_3 \right) \mathrm{d}X_3 \tag{54}$$

$$+ \left[\sum_{A\in P(C)} w^A \delta V \cdot \boldsymbol{\sigma}^{-1} \left(\bar{r} V + \bar{J}\right) \right]_0^L. \tag{55}$$

Note a discrepancy between the mass matrices: the mechanical mass matrix has the density, while the thermal does not. This is because the implementation requires constant mass matrices. The $\frac{\partial u_{strain}}{\partial T}$ term present in the thermal mass is dependent on the mechanical state, so the thermal mass density is divided to place it on the right hand side, where it appears in the denominator in $\mathbb{F}_T$.

4.3. Organization of mixed function spaces

The FEniCS framework is able to build tangents of variational forms automatically. To build the tangents desired, mixed function spaces are defined differently depending on the solution method to be used. Each split equation to be handled by DAE solver is assigned a single mixed function space corresponding to the unknown fields in the equation.

The following definitions correspond directly to the declaration of the mixed function spaces and corresponding solution functions, test functions, and trial functions in FEniCS.

First, in the staggered implicit and explicit cases, the three equations are split, so that three function spaces are needed. The beam fields are grouped into one function space,

$$\mathcal{M}_{beam} = \left\{V_r, \mathcal{V}_g, \mathcal{V}_g\right\} \tag{56}$$

leading to the definition of the following nine-component functions for x, v, δx, and $\dot{v}$:

$$x = \{\mathbf{r}, \mathbf{g}_1, \mathbf{g}_2\} \in \mathcal{M}_{beam} \tag{57}$$

$$v = \left\{\mathbf{vr}, \mathbf{vg}_1, \mathbf{vg}_2\right\} \in \mathcal{M}_{beam} \tag{58}$$

$$\delta x = \{\delta\mathbf{r}, \delta\mathbf{g}_1, \delta\mathbf{g}_2\} \in \mathcal{M}_{beam} \tag{59}$$

$$\dot{v} = \left\{\dot{\mathbf{vr}}, \dot{\mathbf{vg}}_1, \dot{\mathbf{vg}}_2\right\} \in \mathcal{M}_{beam}. \tag{60}$$

These represent the finite element solution space of the mechanical problem, with the additional strongly-enforced condition $\dot{x} = v$. The scalar function spaces for the temperature and velocity listed above are used to complete the description for these cases. The above variational forms form the three equations

$$\mathbb{M}_m\left(\delta x, \dot{v}\right) = \mathbb{F}_m\left(\delta x, v, x, T, V\right) \quad \forall \delta x \in \mathcal{M}_{beam} \tag{61}$$

$$\mathbb{M}_T\left(\delta T, \dot{T}\right) = \mathbb{F}_T\left(\delta T, v, x, T, V\right) \quad \forall \delta T \in S_T \tag{62}$$

$$0 = \mathbb{G}_V\left(\delta V, v, x, T, V\right) \quad \forall \delta V \in S_V. \tag{63}$$

For the monolithic implicit solution, all of the fields are solved simultaneously, and thus one mixed function space is defined as

$$\mathcal{M}_{all} = \left\{\mathcal{V}_r, \mathcal{V}_g, \mathcal{V}_g, \mathcal{S}_T, \mathcal{S}_V\right\}. \tag{64}$$

A trick used is to model the entire system as a rank-deficient second order system in time. The fields are organized together to define the functions y, w, δw and $\dot{w}$ as

$$\{\mathbf{r}, \mathbf{g}_1, \mathbf{g}_2, \emptyset, \emptyset\} = y \in \mathcal{M}_{all} \tag{65}$$

$$\left\{\mathbf{vr}, \mathbf{vg}_1, \mathbf{vg}_2, T, V\right\} = w \in \mathcal{M}_{all} \tag{66}$$

$$\left\{\delta\mathbf{vr}, \delta\mathbf{vg}_1, \delta\mathbf{vg}_2, \delta T, \delta V\right\} = \delta w \in \mathcal{M}_{all} \tag{67}$$

$$\left\{\dot{\mathbf{vr}}, \dot{\mathbf{vg}}_1, \dot{\mathbf{vg}}_2, \dot{T}, \emptyset\right\} = \dot{w} \in \mathcal{M}_{all}. \tag{68}$$

The functions y and w are constrained by the strongly enforced condition $\dot{y} = w$. The velocity fields are considered the primary fields so that the mechanical and thermal mass matrices are in the same form. The nulls, $\emptyset$, are place holders in the finite element function space that are not included in variational form. These are here for convenience in the implementation and will leave behind zero rows and columns in matrices and vectors after assembly. There is only a storage cost in the y vector associated with the null fields in the final program. The variational forms are summed together,

$$\mathbb{M}_{all}\left(\delta w, \dot{w}\right) = \mathbb{M}_m\left(\delta v, \dot{v}\right) + \mathbb{M}_T\left(\delta T, \dot{T}\right) \tag{69}$$

$$\mathbb{F}_{all}\left(\delta w, w, y\right) = \mathbb{F}_m\left(\delta v, v, y, T, V\right) + \mathbb{F}_T\left(\delta T, v, y, T, V\right) + \mathbb{G}_V\left(\delta V, v, y, T, V\right) \tag{70}$$

so that variational statement for the monolithic solution of the problem is

$$\mathbb{M}_{all}\left(\delta w, \dot{w}\right) = \mathbb{F}_{all}\left(\delta w, w, y\right) \quad \forall \delta w \in \mathcal{M}_{all}. \tag{71}$$

5. Time stepping

With the implicit electromagnetic problem, it is not possible to use a purely explicit time marching scheme. This leaves three options for solving the state of the system at the next time step:

1. explicit/implicit splitting: march the dynamics explicitly, solving the implicit problems at each stage;
2. implicit time stepping with staggered iteration: solve each field implicitly, and iterate through the fields one by one until the solution converges; and
3. implicit time stepping with monolithic solution: solve all of the fields simultaneously with a single nonlinear newton iteration.

The first of these methods was used in previous work for a network model in Queiruga [24]. The methodology is similar to solving the pressure–velocity differential algebraic equation for explicit solutions to the incompressible Navier–Stokes [25]. The second is employed in a similar network model in Zohdi [26,27].

The differential algebraic equation can be written in two forms. In this discussion, it does not matter what method was used to discretize the PDEs so that $\mathbf{x}$, $\mathbf{v}$, T and V are treated arrays of discrete values. Here, the arrays are coefficients to finite element functions, where the arrays $\mathbf{x}$ and $\mathbf{v}$ actually refer the coefficients to the beam directors instead of those of a nodal basis. The matrices and vectors $\mathbf{M}_m$, $\mathbf{M}_T$, $\mathbf{F}_m$, $\mathbf{F}_T$ and $\mathbf{G}_V$ are the result of the assembly of the finite element forms described in the previous section. The semi-explicit structure can be shown explicitly by writing it as

$$\begin{aligned} \dot{\mathbf{v}} &= \mathbf{M}_m^{-1}\mathbf{F}_m\left(t, \mathbf{v}, \mathbf{x}, T, V\right) \\ \dot{T} &= \mathbf{M}_T^{-1}\mathbf{F}_T\left(t, \mathbf{v}, \mathbf{x}, T, V\right) \\ 0 &= \mathbf{G}_V\left(t, \mathbf{v}, \mathbf{x}, T, V\right) \end{aligned} \tag{72}$$

where in the actual implementation the mass matrices would not be inverted. For the DAE to be semi-explicit, it must be possible to solve $\mathbf{G}_V$ for the implicit variable V, required that the derivative $\frac{\partial \mathbf{G}_V}{\partial V}$ be nonsingular. The formulation above satisfies this requirement. The fields $\mathbf{v}$, $\mathbf{x}$ and T will be referred to as the "ODE" fields in the following discussion to reflect the fact that their time derivatives appear in the equation. The field V will be referred to as the "implicit" field.

The problem can be written in a more general form,

$$\mathbf{M}_{all}\dot{w} = \mathbf{F}_{all}\left(t, w, y\right) \tag{73}$$

where w and y are new variables that contains all of the unknown fields as described in Eqs. (65) and (66). For the system to be a DAE and not reduce into an ODE, $\mathbf{M}$ must be singular, i.e. rank deficient. In the above example, rows and columns of the mass matrix corresponding to the implicit variable V are zero. The terms $\mathbf{M}_{all}$ and $\mathbf{F}_{all}$ are constructed by concatenating the single field terms in Eq. (72) as so:

$$\mathbf{M}_{all} = \begin{bmatrix} \mathbf{M}_m & 0 & 0 \\ 0 & \mathbf{M}_T & 0 \\ 0 & 0 & 0 \end{bmatrix}, \qquad \mathbf{F}_{all} = \begin{Bmatrix} \mathbf{F}_m \\ \mathbf{F}_T \\ \mathbf{G}_V \end{Bmatrix}. \tag{74}$$

Expressing the DAE in this form is very useful for automatically generating the required forms using a DSL system such as FEniCS.

The initial conditions of $\mathbf{x}\left(t=0\right)$, $\mathbf{v}\left(t=0\right)$, and $T\left(t=0\right)$ are required to fully define the problem. The initial quasistatic field $V\left(t=0\right)$ is not required to be specified because it can be obtained by solving $0 = \mathbf{G}_V\left(\mathbf{x}_0, \mathbf{v}_0, T_0, V_0\right)$ due to the semi-explicit structure of the DAE.

In ODE analysis, the standard trick is to reduce higher-order derivatives into a system of first-order equations by introducing variables and equations such as $\dot{\mathbf{x}} = \mathbf{v}$ [28]. Consider the case where the second order problem is a structural problem, where $\mathbf{x}$ and $\mathbf{v}$ are each vector fields, and the first order and quasistatic component are both scalar fields. The total amount of degrees of freedom to be marched in time is $3N+3N+1N+1N = 8N$. The majority of the degrees of freedom are associated with the discretization of $\mathbf{x}$ and $\mathbf{v}$, so is therefore desirable to treat the second order component specially to decrease the size of the matrix system to be solved (from $8N$ to $5N$ in the given example).

5.1. Runge–Kutta system of equations

For general Runge–Kutta methods marching a first-order ODE $\frac{d\mathbf{u}}{dt} = f\left(\mathbf{u}\right)$, the intermediate stage derivatives, $\mathbf{k}_i$ and the updated value $\mathbf{u}_N = \mathbf{u}\left(t+h\right)$ are calculated starting from $\mathbf{u}_0 = \mathbf{u}\left(t\right)$ by using the equations

Algorithm 1 Explicit Runge–Kutta with quasistatic field

1. Loop over stages, $i = 1, 2, ..., s$
   (a) Compute stage values for all ODE fields using Equations 75, 76, and $\mathbf{x}_i = \mathbf{x}_0 + h \sum_{j<s} a_{ij} \mathbf{v}_j$.
   (b) Newton's method to solve V_i using Equation 78.
   (c) Calculate and save $\mathbf{k}_i$ for each ODE field:
   $\mathbf{k}_{mi} = \mathbf{F}_m (\mathbf{x}_i, \mathbf{v}_i, T_i, V_i)$
   $\mathbf{k}_{Ti} = \mathbf{F}_T (\mathbf{x}_i, \mathbf{v}_i, T_i, V_i)$
2. Final recombination step using Equations 79, 80 and 81.
3. Newton's method to solve Equation 82 for $V(t + h)$ with Equation 78.

Algorithm 2 Implicit Runge–Kutta with staggered solution

1. Loop over stages, $i = 1, 2, ..., s$
   (a) Perform staggering iteration, $I = 1, 2, ...$
      i. Newton's method for $\mathbf{x}_i^I$ and $\mathbf{v}_i^I$ using Equation 86.
      ii. Newton's method for T_i^I using Equation 87.
      iii. Newton's method for V_i^I using Equation 88.
      iv. Repeat for $I = I + 1$ if Steps i,ii, or iii required more than one iteration
   (b) Store last computed $\mathbf{k}$ values
2. Perform final recombination step using Equations 79, 80 and 81.
3. Newton's method to solve Equation 82 for $V(t + h)$ with Equation 78.

Algorithm 3 Implicit Runge–Kutta with monolithic solution

1. Loop over stages, $i = 1, 2, ..., s$
   (a) Newton's method for w_i and y_i using Equation 90.
   (b) Store last computed $\mathbf{k}$ values

(Method only implemented for $c_s = 1$, no final step needed)

$\mathbf{k}_i = f\left(\mathbf{u}_0 + h \sum_{j=1}^{s} a_{ij} \mathbf{k}_j\right)$ and $\mathbf{u}_N = \mathbf{u}_0 + h \sum_{i=1}^{s} b_i \mathbf{k}_i$, where s is the number of stages and $i = 1, 2, \ldots, s$. The general scheme is modified to handle the second order and quasistatic components.

The second order system has a trivial equation $\frac{d\mathbf{x}}{dt} = \mathbf{v}$. Marching the trivial component first, each stage of the position is related to the previous stage values and current stage value of the velocity by $\mathbf{x}_i = \mathbf{x}_0 + h \sum_{j<s} a_{ij} \mathbf{v}_j$. This solution is plugged directly into the other equations to eliminate the need to solve for x_i independently. For the other equations in the system to be satisfied for the current stage, $\mathbf{v}_i$, T_i and V_i must satisfy

$$\mathbf{M}_m \mathbf{v}_i = \mathbf{M}_m \mathbf{v}_0 + h \sum_{j=1}^{i} a_{ij} \mathbf{F}_m \left(\mathbf{x}_0 + h \sum_{k=1}^{j} a_{jk} \mathbf{v}_k, \mathbf{v}_j, T_j, V_j \right) \tag{75}$$

$$\mathbf{M}_T T_i = \mathbf{M}_T T_0 + h \sum_{j=1}^{i} a_{ij} \mathbf{F}_T \left(\mathbf{x}_0 + h \sum_{k=1}^{i} a_{ik} \mathbf{v}_k, \mathbf{v}_j, T_j, V_j \right) \tag{76}$$

$$0 = \mathbf{G}_V \left(\mathbf{x}_0 + h \sum_{k=1}^{i} a_{ik} \mathbf{v}_k, \mathbf{v}_i, T_i, V_i \right) \tag{77}$$

5.2. Semi-explicit splitting

In an explicit method, only the previous stage values of the fields are needed for the current stage evaluation. The quasistatic field needs to be solved implicitly at each stage, but the ODE fields can be marched explicitly. Whenever a derivative evaluation is required for the ODE fields, the quasistatic field V is solved. At each intermediate stage i, the

problem $0 = \mathbf{G}_V\left(\mathbf{x}_i, \mathbf{v}_i, T_i, V_i\right)$, can be solved for V_i because $\mathbf{x}_i$, $\mathbf{v}_i$, and T_i have been specified by Eqs. (75) and (76). The following Newton's method iteration is used to solve the nonlinear problem

$$0 = \left[\left.\frac{\partial \mathbf{G}_V}{\partial V}\right|_{\mathbf{x}_i, \mathbf{v}_i, T_i, V^{[k]}}\right] \Delta V^{[k]} + \mathbf{G}_V\left(\mathbf{x}_i, \mathbf{v}_i, T_i, V_i^{[k]}\right) \tag{78}$$

where k is the iteration variable, $V^{[k]}$ is the intermediate value, and $\Delta V^{[k]}$ is the Newton update to obtain $V^{[k+1]} = V^{[k]} + \Delta V^{[k]}$. The initial value of the iteration is set to the previously calculated stage value of V_{i-1}.

Typically, a lumped mass approximation is used so that the matrix solution is not required at each derivative evaluation. However, this results in the scheme solving a slightly different problem, so the consistent mass matrix is used in this work to allow the numerical comparison between the explicit and implicit methods. The Dirichlet boundary conditions on the ODE fields need to be applied on linear systems involving mass matrices, e.g. $\mathbf{M}_m \mathbf{v}_i = \mathbf{R}$.

The mass matrix must also be used for the last linear combination,

$$\mathbf{M}_m\left(\mathbf{v}_N - \mathbf{v}_0\right) = h \sum_{i=1}^{s} b_i \mathbf{k}_{mi} \tag{79}$$

$$\mathbf{M}_T\left(T_N - T_0\right) = h \sum_{i=1}^{s} b_i \mathbf{k}_{Ti}. \tag{80}$$

The second order field is similarly determined using the stage velocities by

$$\mathbf{x}_N = \mathbf{x}_0 + h \sum_{i=1}^{s} b_i \mathbf{v}_i. \tag{81}$$

Because the implicit field is not satisfied after this step, the implicit equation must be solved again for V_N,

$$0 = \mathbf{G}_V\left(\mathbf{x}_N, \mathbf{v}_N, T_N, V_N\right), \tag{82}$$

at the end of time step.

5.3. Implicit stepping

Diagonally implicit Runge–Kutta schemes are used, allowing the nonlinear problem of each stage to solve independently with only N-unknowns. Both L-stable and not L-stable methods are used. For the L-stable schemes, the final stage in these methods is at $t + h$ (i.e., $c_s = 1$) and the final row in A_{ij} is equal to b_j,[3] and so the nonlinear solution step gives $x\left(t + h\right)$, $T\left(t + h\right)$, and $V\left(t + h\right)$ without any extra work. When $c_s \neq 1$, the mass matrix can be back-solved with the linear combination to determine the values at $t + h$, but the quasi-static field requires performing an extra solution step.

For convenience, let the following symbols represent the current stage value minus the diagonal component (i.e., the unknown term): $\hat{\mathbf{v}}_i = \mathbf{v}_0 + h\sum_{j<i} a_{ij}\mathbf{F}_{mj}$, $\hat{\mathbf{x}}_i = \mathbf{x}_0 + h\sum_{j<i} a_{ij}\mathbf{v}_j$, and $\hat{T}_j = T_0 + h\sum_{j<i} a_{ij}\mathbf{F}_{Tj}$. Breaking the stage summations into the diagonal and lower triangular components to group together terms that depend on the current stage, the nonlinear system of equations

$$\mathbf{M}_m\mathbf{v}_i - h a_{ii}\mathbf{F}_m\left(\hat{\mathbf{x}}_i + h a_{ii}\mathbf{v}_i, \mathbf{v}_i, T_i, V_i\right) = \mathbf{M}_m\mathbf{v}_0 + h\sum_{j<i} a_{ij}\mathbf{F}_m\left(\mathbf{x}_j, \mathbf{v}_j, T_j, V_j\right) \tag{83}$$

$$\mathbf{M}_T T_i - h a_{ii}\mathbf{F}_T\left(\hat{\mathbf{x}}_i + h a_{ii}\mathbf{v}_i, \mathbf{v}_i, T_i, V_i\right) = \mathbf{M}_T T_0 + h\sum_{j<i} a_{ij}\mathbf{G}_V\left(\mathbf{x}_j, \mathbf{v}_j, T_j, V_j\right) \tag{84}$$

$$\mathbf{G}_V\left(\hat{\mathbf{x}}_i + h a_{ii}\mathbf{v}_i, \mathbf{v}_i, T_i, V_i\right) = 0 \tag{85}$$

is obtained, with all unknown values placed on the left side. Using the chain rule, the linearization of one of the functions on the left hand side with respect to $\mathbf{v}_i$ is $\frac{\partial}{\partial \mathbf{v}_i} = h a_{ii}\frac{\partial}{\partial \mathbf{x}} + \frac{\partial}{\partial \mathbf{v}}$. This is used to form Newton's method iterations for the second order fields.

[3] This property actually implies L-stability; see Alexander, 1997 [29] for a proof.

5.3.1. Staggered field iteration

The three equations above can be solved in a decoupled manner by solving each field independently with the others frozen and iterating between the equations until the process has converged. The following three Newton's method iterations are used for each field, with $[k]$ denotes the current value, and $\tilde{()}_i$ denotes the current values of the frozen fields. The velocities are iteratively updated using the linear system of equations

$$\left[\mathbf{M}_m - h^2 a_{ii}^2 \frac{\partial \mathbf{F}_m}{\partial \mathbf{x}} - h a_{ii} \frac{\partial \mathbf{F}_m}{\partial \mathbf{v}}\right] \Delta \mathbf{v}^{[k]} = \mathbf{M}_m \mathbf{v}_0 + h \sum_{j=1}^{i-1} a_{ij} \mathbf{F}_m \left(\mathbf{v}_j, \mathbf{x}_j, T_j, V_j\right) - \mathbf{M}_m \mathbf{v}_i^{[k]} + h a_{ii} \mathbf{F}_m \left(\mathbf{v}_i^{[k]}, \mathbf{x}_i^{[k]}, \tilde{T}_i, \tilde{V}_i\right). \tag{86}$$

The update for the second order field is applied to both $\mathbf{v}_i^{[k+1]} = \mathbf{v}_i^{[k]} + \Delta \mathbf{v}^{[k]}$, and $\mathbf{x}_i^{[k]} = \mathbf{x}_i^{[k]} + h a_{ii} \Delta \mathbf{v}^{[k]}$. The first-order temperature field requires solving

$$\left[\mathbf{M}_T - h a_{ii} \frac{\partial \mathbf{F}_T}{\partial T}\right] \Delta T^{[k]} = \mathbf{M}_T T_0 + h \sum_{j=1}^{i-1} a_{ij} \mathbf{F}_T \left(\mathbf{v}_j, \mathbf{x}_j, T_j, V_j\right) - \mathbf{M}_T T_i^{[k]} + h a_{ii} \mathbf{F}_T \left(\tilde{\mathbf{x}}_i, \tilde{\mathbf{v}}_i, T_i^{[k]}, \tilde{V}_i\right) \tag{87}$$

for ΔT, with the similar update $T_i^{[k+1]} = T_i^{[k]} + \Delta T^{[k]}$. Finally, the implicit equation must be satisfied for the stage values, so the following equation

$$0 = \left[\left.\frac{\partial \mathbf{G}_V}{\partial V}\right|_{\tilde{\mathbf{x}}, \tilde{\mathbf{v}}, \tilde{T}, V^{[k]}}\right] \Delta V^{[k]} + \mathbf{G}_V \left(\tilde{\mathbf{x}}_i, \tilde{\mathbf{v}}_i, \tilde{T}_i, V_i^{[k]}\right) \tag{88}$$

is used to determine V_i via the iteration $V_i^{[k+1]} = V_i^{[k]} + \Delta V^{[k]}$. With most methods for PDE discretization, all of the matrices that need to be solved will be symmetric.

5.3.2. Monolithic solution

Consider now the form of the DAE in Eq. (73), where the fields w and y are defined by grouping the individual fields in the form of Eqs. (66) and (65). The subscript "*all*" on $\mathbf{M}$ and $\mathbf{F}$ is dropped in this section. Following the same methodology as in the case above, applying the scheme to y and plugging $y_i = y_0 + h \sum_{j<i} a_{ij} w_j + h a_{ii} w_i$ into equation for w_i yields a similar form of

$$\mathbf{M} w_i - h a_{ii} \mathbf{F} \left(w_i, y_0 + h \sum_{k=1}^{i} a_{ik} w_k + h a_{ii} w_i\right) = \mathbf{M} w_0 + h \sum_{j=1}^{i-1} a_{ij} \mathbf{F} \left(w_j, y_j\right). \tag{89}$$

The entire system can be linearized at once about $w_i^{[k]}$ in the direction Δw, which simultaneously linearizes in the direction $\{\Delta \mathbf{v}, \Delta T, \Delta V\}$, to make the Newton iteration:

$$\left(\mathbf{M} - h a_{ii} \frac{\partial \mathbf{F}}{\partial w} - h^2 a_{ii}^2 \frac{\partial \mathbf{F}}{\partial y}\right) \Delta w = \mathbf{M} w_0 + h \sum_{j=1}^{i-1} a_{ij} \mathbf{F} \left(w_j, y_j\right) - \mathbf{M} w_i^{[k]} + h a_{ii} \mathbf{F} \left(w_i^{[k]}, y_i^{[k]}\right). \tag{90}$$

The derivatives of the monolithic $\mathbf{F}$ can be constructed in terms of the individual equations by

$$\frac{\partial \mathbf{F}}{\partial w} = \begin{bmatrix} \frac{\partial \mathbf{F}_m}{\partial \mathbf{v}} & \frac{\partial \mathbf{F}_T}{\partial \mathbf{v}} & \frac{\partial \mathbf{G}_V}{\partial \mathbf{v}} \\ \frac{\partial \mathbf{F}_m}{\partial T} & \frac{\partial \mathbf{F}_T}{\partial T} & \frac{\partial \mathbf{G}_V}{\partial T} \\ \frac{\partial \mathbf{F}_m}{\partial V} & \frac{\partial \mathbf{F}_T}{\partial V} & \frac{\partial \mathbf{G}_V}{\partial V} \end{bmatrix}, \qquad \frac{\partial \mathbf{F}}{\partial y} = \begin{bmatrix} \frac{\partial \mathbf{F}_m}{\partial \mathbf{x}} & \frac{\partial \mathbf{F}_T}{\partial \mathbf{x}} & \frac{\partial \mathbf{G}_V}{\partial \mathbf{x}} \\ \mathbf{0} & \mathbf{0} & \mathbf{0} \\ \mathbf{0} & \mathbf{0} & \mathbf{0} \end{bmatrix}. \tag{91}$$

The rows of $\mathbf{M}$ and $\frac{\partial \mathbf{F}}{\partial y}$ corresponding to $\emptyset$ field placeholders are zero after the calculations are carried out. The linearized parts of the quasistatic equations appear in $\frac{\partial \mathbf{F}}{\partial w}$.

Table 2
Dynamic problem parameters.

Simulation duration t_{max}	2.5 ms	Young's modulus E	10 MPa
Length L	1 mm	Temperature coefficient $\alpha_\mu, \alpha_\lambda$	$-0.1\ \frac{\text{MPa}}{\text{K}}, 0\ \frac{\text{MPa}}{\text{K}}$
Wire radius R	0.02 mm	Electric conductivity σ	$1\ \frac{\text{S}}{\text{mm}}$
Magnetic field magnitude B	1 T	Seebeck coefficient S	$0.1\ \frac{\text{V}}{\text{K}}$
Magnetic field angle ϕ	$\frac{\pi}{4}$	Resistance BC $\bar{r}$	$0.5\ \frac{\text{S}}{\text{mm}}$
Dissipation γ	$0.01\ \frac{\text{Ns}}{\text{m}}$	Applied current BC $\bar{J}$	1 A
Heat capacity c_v	$1.0\ \frac{\text{mJ}}{\text{K}}$	Density ρ	$1\ \frac{\text{g}}{\text{mm}^3}$

The difference between construction by concatenating matrices and assembling using a monolithic function space as specified in Eq. (64) is the ordering of the unknowns: the finite element implementation is now free to automatically order the unknown fields. This results in a $\{x, y, z, T, V, x, y, z, T, V, \ldots\}$ ordering instead of a $\{x, x \ldots y, y \ldots z, z \ldots T, T \ldots V, V \ldots\}$ ordering, greatly reducing the bandwidth of the linear systems.

The implementation of the monolithic system makes it difficult to perform the final linear combination step and quasistatic solution, so only L-stable methods that do not require this step are used.

6. Implementation details

The code is built in the Python programming language and is dependent upon the finite element package FEniCS [17]. The Python code uses a number of C++ extensions which are interfaced as submodules. The code also makes use of Numpy [30] and Scipy [31] for the de facto standard Python numerical array data type and numerical algorithms; Mathematica [32] for code generation and symbolic integration and differentiation; Matplotlib [33] for plotting; and Paraview [34] for visualization. The Runge–Kutta time stepping logic is entirely written in Python using the low-level optimized vector and matrix operations of Numpy and FEniCS. The staggered and monolithic solution schemes use the same implementation. A monolithic solution is set up by inputting a single-second order field with a rank deficient mass matrix $\mathbf{M}$ into the general implicit Runge–Kutta routine. Because there is only one field in the list of fields, no staggering iteration occurs.

7. Results and discussion

7.1. Model problem

The model problem is an initially straight cylindrical beam with uniform initial temperature with both ends clamped. The beam is suddenly connected to the circuit described in Fig. 1 at $t = 0$. The clamps remain fixed, and the electric current varies due to the motion of the beam inducing a back electromotive force. The parameters used for this simulation are shown in Table 2. The temperature change is pinned to 0 at the endpoints, the normalized reference temperature. For the voltage boundary conditions, the side at $-L$ is held at ground (0 V), and the mixed boundary condition of Eq. (25) is applied to the other side with the values in Table 2. The values were chosen so that the voltage drop across the beam is 1 V at rest and the external resistor has the same resistance as the beam itself. The magnetic field is oriented in the xy plane at an angle ϕ to the initial state of the beam to induce a helical bending.

The beam is discretized in space using forty elements and all of fields have linear basis functions. Since there is no known analytical solution, even an approximate one, for comparison, the spatial discretization is not important and is kept low to decrease the computational cost of each time step. Four locations are probed in the solution: (1) the vertical displacement at the center, $y\,(X_3 = 0)$; (2) the lateral displacement a quarter of the way through the beam, $z\,(X_3 = 1/2)$; (3) the temperature a quarter of the way through the beam, $T\,(X_3 = 1/2)$; and (4) the voltage a quarter of the way through the beam, $V\,(X_3 = 1/2)$. Only the first probe is placed at the center because the symmetry of solution causes uninteresting behavior in the other fields at that point. The deformation and current field of the beam are rendered in Fig. 5 and the fields probed are plotted in time in Fig. 6. As can be seen in Fig. 5, the current magnitude is not uniform along the beam at each point in time due to the Seebeck effect and nonuniform electromotive force.

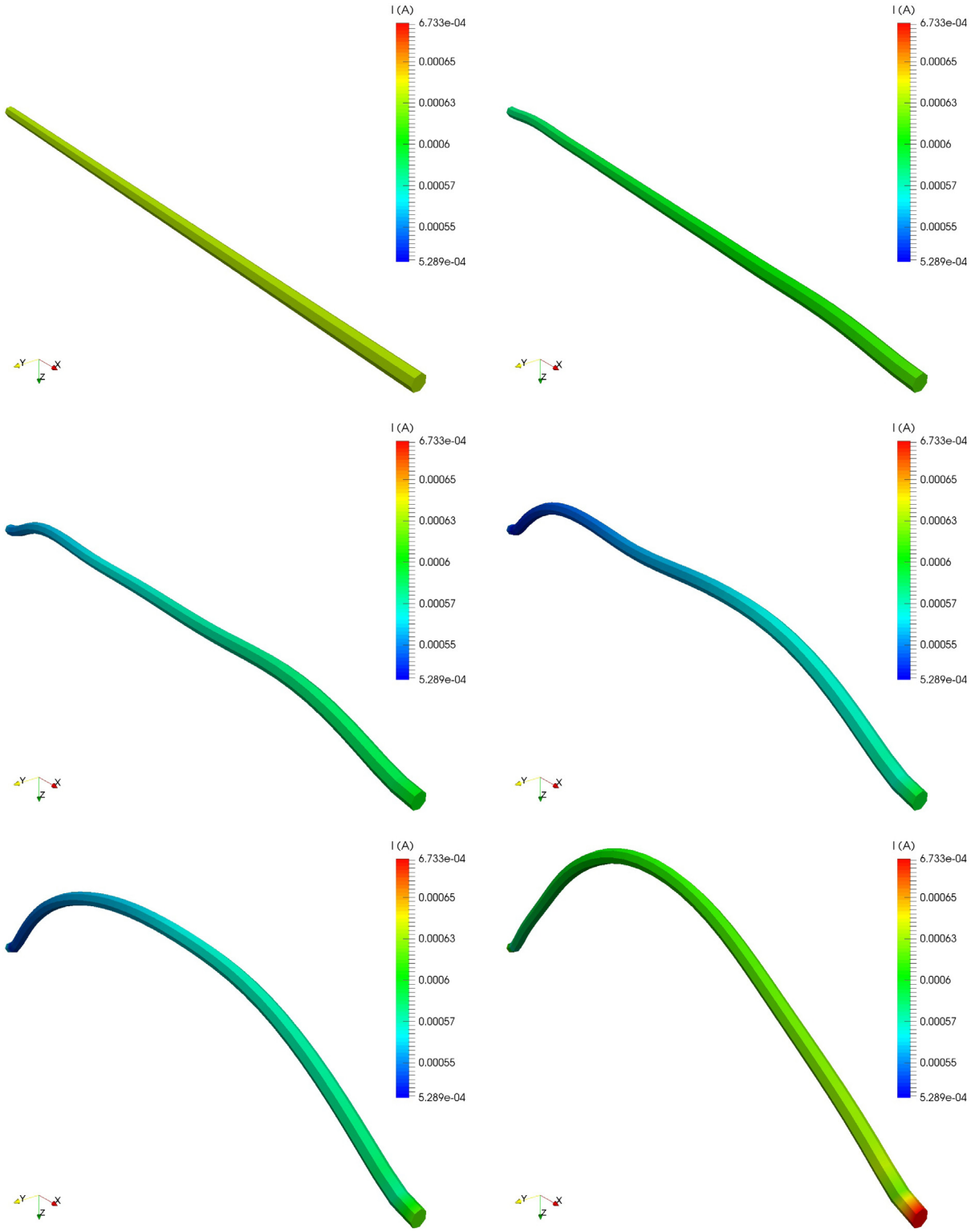

Fig. 5. Time series of the model problem with frames spaced equally apart. The mesh is colored by the current magnitude, measured in amperes, with the same ranging in each frame. The current magnitude is not uniform along the beam at each point in time due to the Seebeck effect and nonuniform electromotive force. The beam deforms in the $-z$ direction; the camera is rotated 180°. (For interpretation of the references to color in this figure legend, the reader is referred to the web version of this article.)

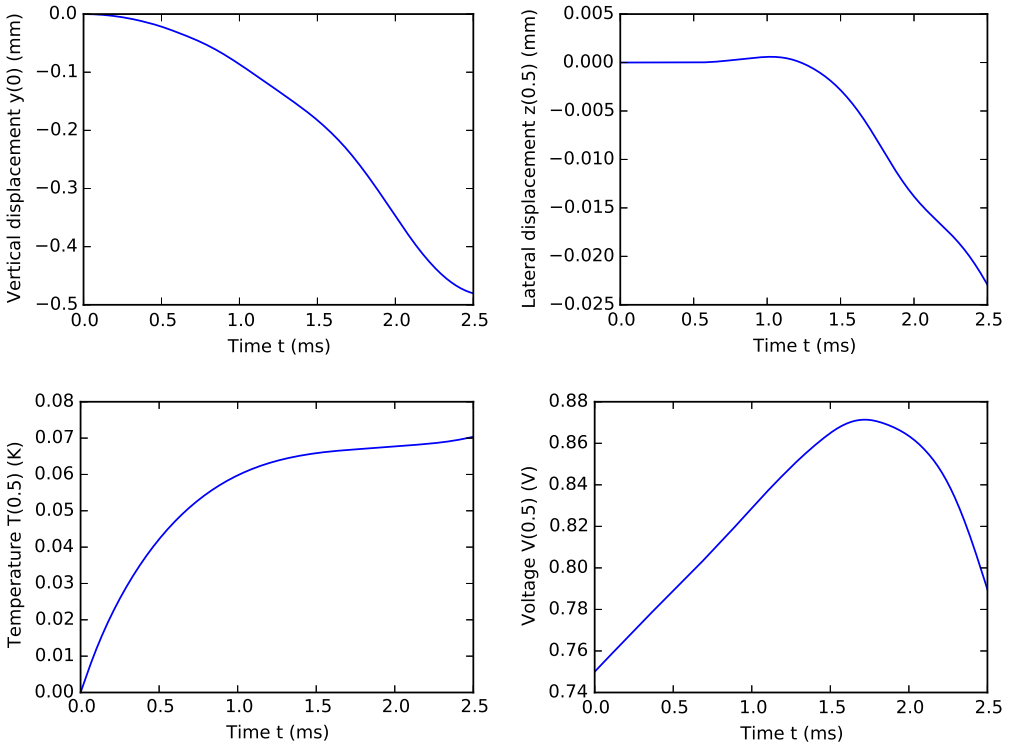

Fig. 6. Time plots of the four probes from the scheme RK4 with $N_t = 10{,}000$.

7.2. Error analysis

Multiple Runge–Kutta methods were used to verify that the numerical solution behaves as expected. The method referred to as "RK2-mid" is two stages and commonly known as the explicit midpoint method with $\mathbf{c} = \left\{0, \frac{1}{2}\right\}$. The label "RK3-1" refers to the three stage explicit scheme with $\mathbf{c} = \left\{0, \frac{2}{3}, \frac{2}{3}\right\}$. The label "RK4" refers to the classical four-stage explicit Runge–Kutta method. The one-stage implicit midpoint method is referred to as "ImMid". The tableaus of the previously mentioned methods can be found in Butcher, 1987 [35]. The two methods labeled "DIRK2" and "DIRK3" have two and three stages, respectively, and are credited to Crouzeix, 1975 [36] and Nørsett, 1974 [37]. The methods "LSDIRK2" and "LSDIRK3" are L-stable schemes derived by Alexander, 1977 [29].

Since there is no available analytical solution for this problem, the solutions are compared to an over-refined case of the classical RK4 method with $N_t = 100{,}000$. The error in all four fields is calculated across the domain. Because the mesh remains the same while varying the time stepping scheme and time step size, the error metric between two fields integrated over the domain is simplified by examining only the coefficients to reduce the post-processing complexity. For each field, called y here, constructed by coefficients $y(\xi_3) = \sum_i a_i \phi_i(\xi_3)$, the L_2 error between the "best" solution, y^{best}, and a given solution y is approximated by the equation

$$e(y) = \frac{\sqrt{\int_\Omega \left(y^{best} - y\right)^2 d\Omega}}{\sqrt{\int_\Omega \left(y^{best}\right)^2 d\Omega}} \approx \frac{\sqrt{\sum_i \left(a_i^{best} - a_i\right)^2}}{\sqrt{\sum_i \left(a_i^{best}\right)^2}}. \tag{92}$$

(This is equivalent to using an inexact nodal quadrature rule to calculate the error integral.) The vector components of a vector field are analyzed together, but the coefficients of the centroid and director fields are analyzed as separate fields, as well as their velocities, so that there are a total of eight errors for a given solution. A single error metric is taken by taking the two-norm of the list of eight errors.

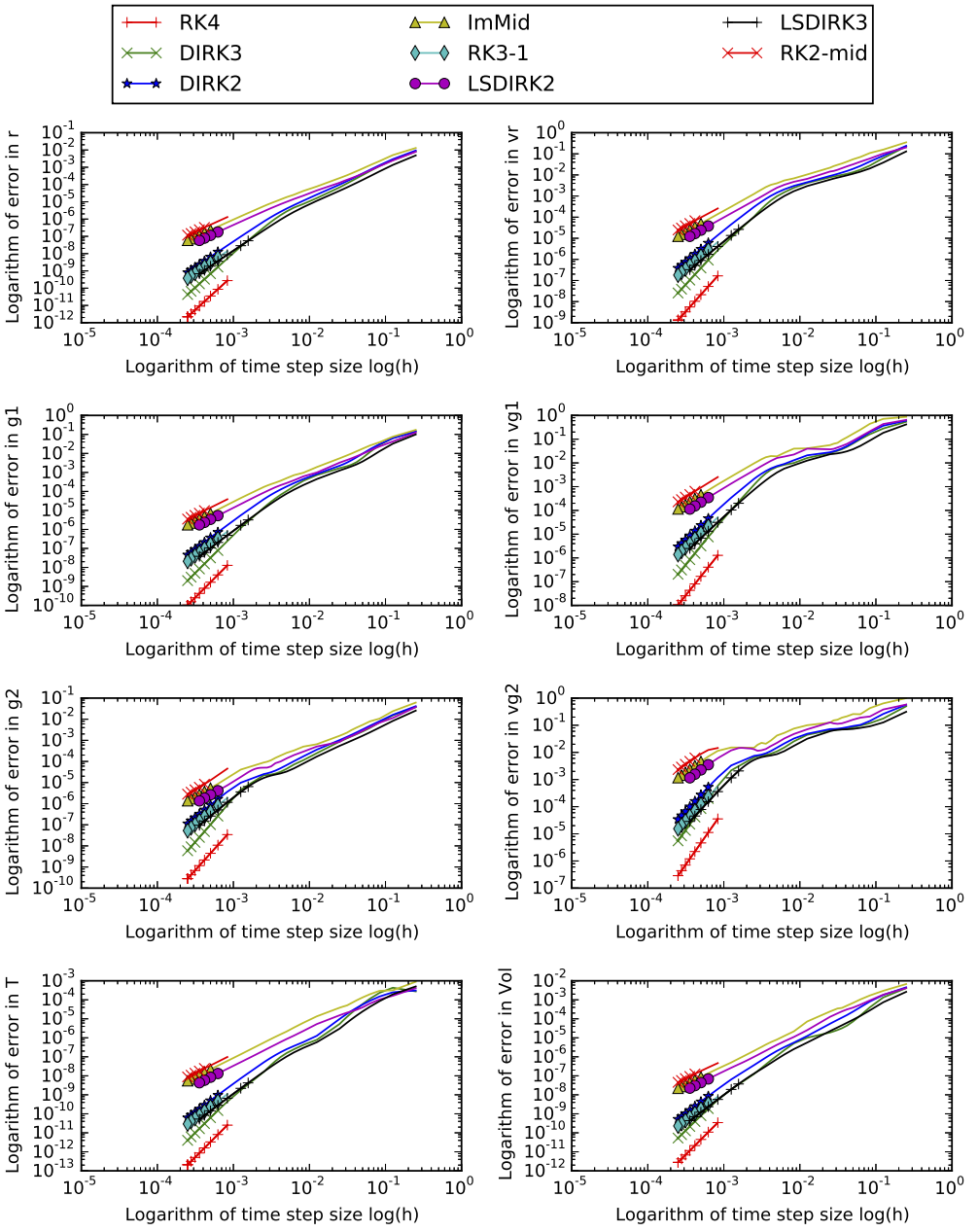

Fig. 7. Obtained errors for all fields independently.

Due to the nonlinear nature of the problem, constructing a setup suitable to test convergence errors is challenging. At the larger time steps that the implicit methods are able to take, the approximate solutions approach a slightly different solution (with an error of about 10^{-4}) than the over-refined solution. The fields $\mathbf{g}_2$ and $\mathbf{vg}_2$, associated with the director in the z-direction, especially suffer from this trend (see Fig. 7). The authors hypothesize that, after a certain duration, Lipschitz continuity breaks down in the problem due to the bifurcations associated with the buckling modes and free-rotation at pinned BCs. To make the problem "easier" for the numerical solver, the timespan of the simulation is kept short and clamped boundary conditions are used. These considerations motivated the choice of parameters in Table 2.

The convergence orders for each of the eight fields separately are shown in Fig. 7. The same time steps were tried for all methods; the smallest time step that converged is shown for each explicit method. The convergence orders

Table 3
Computed convergence orders.

Method	Expected	Observed	Method	Expected	Observed
RK2-mid	$\mathcal{O}\left(h^2\right)$	1.949	DIRK2	$\mathcal{O}\left(h^3\right)$	2.990
RK3-1	$\mathcal{O}\left(h^3\right)$	2.969	DIRK3	$\mathcal{O}\left(h^4\right)$	3.916
RK4	$\mathcal{O}\left(h^4\right)$	4.000	LSDIRK2	$\mathcal{O}\left(h^2\right)$	1.988
ImMid	$\mathcal{O}\left(h^2\right)$	1.985	LSDIRK3	$\mathcal{O}\left(h^3\right)$	2.953

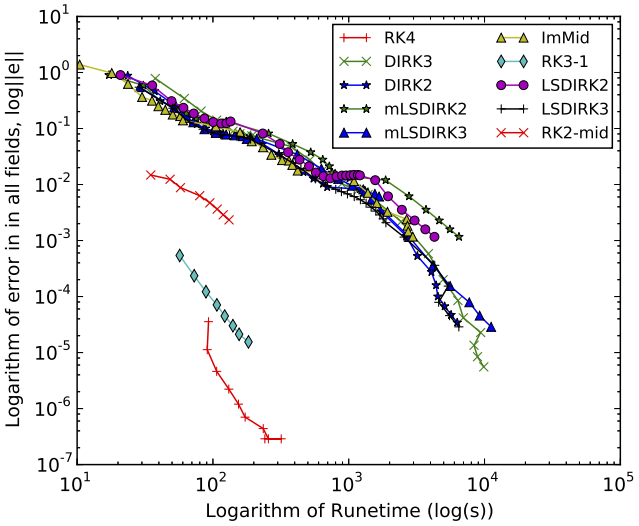

Fig. 8. Runtimes of methods required to produce a desired error plotted in a log–log scale. The methods prefixed by "m" were solved monolithically.

were computed with the points marked by crosses. The two-norm of the set of eight fields was used for the order calculation, and the results are listed in Table 3. All methods produced the expected convergence orders.

7.3. Runtime

The methods were analyzed for performance using a simple process-time timing (as opposed to wall-time). Since only a rough comparative metric was desired, the program was run single-threaded on a 2013 Macbook Pro laptop with a 2.9 GHz Intel Core i7. The problem setup was designed to perform all of the tests in one day of computation time. The resulting runtimes are plotted in Fig. 8. The three explicit methods used are able to produce a high-accuracy solution much faster than any of the implicit methods. The only advantage to the implicit methods is the ability to produce a low accuracy solution in a short time using large time steps. The methods solved by both staggered solution and monolithic solution are also shown in the plot, with the labels "LSDIRK2", "LSDIRK3" for the staggered solution scheme, and "mLSDIRK2" and "mLSDIRK3" for the monolithic solution scheme. The staggered iteration is overall faster than the monolithic solution for smaller time steps and higher accuracy. For very large time steps, the monolithic solution for LSDIRK2 is faster. The number of iterations used in the staggering iterations decreases with the size of the time step: at large time steps, about eight coupling iterations are required, while for smaller time steps, only about four coupling iterations are needed.

The code was profiled at the Python level using the library line_profiler by Robert Kern (which can be found at https://github.com/rkern/line_profiler) to observe where the different schemes were spending the bulk of the computation. The break downs are shown in Table 4. The explicit method was RK4 with 1000 time steps, and the implicit methods were LSDIRK3 with 100 time steps. Some categories are merged in the methods: In the

Table 4
Computational cost breakdowns as a percentage of total runtime obtained from profiling. Ditto marks denote categories that could not be discerned due to code structure.

	Explicit	Staggered Imp.	Monolithic Imp.
Assembly of $\mathbf{F}_m$	26.0%	89.8%	96.8%
Assembly of $\mathbf{F}_T$	"	1.0%	"
Assembly of $\mathbf{G}_V$	14.2%	0.6%	"
Solving $\mathbf{M}$	24.8%	6.3%	1.1%
Solving $\mathbf{G}_V$	6.6%	"	"
Misc. Overhead	28.4%	2.3%	2.1%

explicit method, the ODE fields are treated by the same code, so assembly of $\mathbf{F}_m$ and $\mathbf{F}_T$ cannot be differentiated. Similarly, all matrix solutions are handled by the same line of code in the implicit methods. In the monolithic solution, all forms are assembled simultaneously. Application of boundary conditions is included in the matrix solution category. The miscellaneous calculations include vector operations for computing the Runge–Kutta stages. The implementation is not well optimized in terms of reusing data structures and allocated regions of memory (e.g., there are a few unnecessary copies, and the sparsity structure of tangent matrices is recomputed every time a new matrix is assembled). The profiling results show that the time spent on these operations is not very significant for the implicit methods, but is significant for the explicit method. Additionally, using the consistent mass matrix imposes a very high cost to the explicit method, where a lumped-mass approximation could yield a significant performance benefit.

8. Conclusion

A formulation for the dynamic analysis of moving current-carrying wires in magnetic fields was developed utilizing both a quasistatic approximation and a thin-beam approximation to simplify the solution of the electromagnetic equations to a one-dimensional implicit PDE along the axis of the wire. The resulting three coupled partial differential equations along the beam were solved using both implicit and explicit higher-order Runge–Kutta methods, with the added handling for the electric potential equation as described.

It is not necessary to use stiffly stable Runge–Kutta methods for the resulting DAE, as both explicit methods and non-stiffly stable implicit methods were effective. Removing the stiff partial differential equation for charge density allows the use of explicit methods with an added implicit-field solution step with tractable time steps. The Runge–Kutta treatment for the DAE described in Section 5 can be applied to other problems with similar structure (and the implementation is also general enough to be used in other problems), though the numerical properties were only studied on the current-carrying beam.

The higher order explicit methods outperform the diagonally implicit methods greatly at high accuracies. The implementation for the explicit methods also has significant room for improvement as overhead costs are significant. Particularly, there is significant cost associated with using a consistent mass matrix, which was only needed to compare numerical accuracy with the implicit methods. However, the implicit methods have the typical advantage of operating at very large time steps at a low computational cost, which may be useful in certain configurations when the stability of the problem restricts the time step size of the explicit methods.

Because the staggered solution for the implicit schemes is faster than the monolithic solution at high accuracy and comparable with low accuracy, the extra effort of formulating the tangents for the cross-field terms (e.g., $\frac{\partial \mathbf{F}_T}{\partial V}$) is avoidable. Formulating the voltage tangent $\frac{\partial \mathbf{G}_V}{\partial V}$ is still necessary to use the explicit method. The implementation of a monolithic iteration was only tractable due to the use of the differentiation package in FEniCS; deriving the equations for cross-field tangent matrix components would not have been attempted if the authors were to do it by hand. The tangent matrix and coupling sources for the Voltage problem alone were implemented much faster using the DSL system than could have been done otherwise.

The discretized model problem is quite small, with only 451 degrees of freedom. The runtime of the implicit methods should be examined on a larger problem with which the additional overheads would be amortized. Current work is considering contacts between multiple current-carrying beams in a textile structure that may make the implicit methods more attractive in comparison to the explicit methods.

Acknowledgment

This work was funded by the Army Research Laboratory through the Army High Performance Computing Research Center (cooperative agreement W911NF-07-2-0027).

References

[1] M.J. Sinclair, A high force low area mems thermal actuator, in: Thermal and Thermomechanical Phenomena in Electronic Systems, 2000. ITHERM 2000. The Seventh Intersociety Conference on, vol. 1, IEEE, 2000.
[2] J. Wright, Y.-C. Tai, S.-C. Chang, et al., A large-force, fully-integrated mems magnetic actuator, in: Solid State Sensors and Actuators, 1997. TRANSDUCERS'97 Chicago., 1997 International Conference on, vol. 2, IEEE, 1997, pp. 793–796.
[3] C.S. Haines, M.D. Lima, N. Li, G.M. Spinks, J. Foroughi, J.D. Madden, S.H. Kim, S. Fang, M.J. de Andrade, F. Göktepe, et al., Artificial muscles from fishing line and sewing thread, Science 343 (6173) (2014) 868–872.
[4] A. Krajewski, K. Magniez, R. Helmer, V. Schrank, Piezoelectric force response of novel 2d textile based pvdf sensors, IEEE Sensors J. 13 (12) (2013) 4743–4748.
[5] K.S. Yee, Numerical solution of initial boundary value problems involving Maxwell's equations in isotropic media, IEEE Sensors J. and Propagation 14 (3) (1966) 302–307.
[6] J.-C. Nédélec, Mixed finite elements in r3, Numer. Math. 35 (3) (1980) 315–341.
[7] U.S. Inan, R.A. Marshall, Numerical Electromagnetics: The FDTD Method, Cambridge University Press, 2011.
[8] M.I. Barham, D.A. White, D.J. Steigmann, Finite element modeling of the deformation of magnetoelastic film, J. Comput. Phys. 229 (18) (2010) 6193–6207.
[9] Z. Ren, B. Ionescu, M. Besbes, A. Razek, Calculation of mechanical deformation of magnetic materials in electromagnetic devices, IEEE Trans. Magn. 31 (3) (1995) 1873–1876.
[10] M. Besbes, Z. Ren, A. Razek, Finite element analysis of magneto-mechanical coupled phenomena in magnetostrictive materials, IEEE Trans. Magn. 32 (3) (1996) 1058–1061.
[11] G. Brandstetter, S. Govindjee, A high-order immersed boundary discontinuous-Galerkin method for Poisson's equation with discontinuous coefficients and singular sources, Internat. J. Numer. Methods Engrg. 101 (11) (2015) 847–869.
[12] G. Brandstetter, A high-order euler-lagrangian finite element method for coupled electro-mechanical systems (Ph.D. thesis), University of California, Berkeley, 2015.
[13] E. Hairer, G. Wanner, Solving ordinary differential equations II: Stiff and differential-algebraic problems, Vol. 14, Springer-Verlag, Berlin, 1996.
[14] C.C. Pantelides, The consistent initialization of differential-algebraic systems, SIAM J. Sci. Stat. Comput. 9 (2) (1988) 213–231.
[15] E.R. Lima, M. Castier, E.C. Biscaia Jr, Differential-algebraic approach to dynamic simulations of flash drums with rigorous evaluation of physical properties, Oil Gas Sci. Technol. 63 (5) (2008) 677–686.
[16] P. Maffezzoni, L. Codecasa, D. D'Amore, Time-domain simulation of nonlinear circuits through implicit Runge–Kutta methods, IEEE Trans. Circuits Syst. I 54 (2) (2007) 391–400.
[17] A. Logg, K.-A. Mardal, G. Wells, Automated Solution of Differential Equations by The Finite Element Method: The FEniCS book, Vol. 84, Springer Science & Business Media, 2012.
[18] A. Logg, K.B. Ølgaard, M.E. Rognes, G.N. Wells, Ffc: the fenics form compiler, in: Automated Solution of Differential Equations by the Finite Element Method, Springer, 2012, pp. 227–238.
[19] A. Kovetz, Electromagnetic Theory, Oxford University Press Oxford, 2000.
[20] D.J. Steigmann, On the formulation of balance laws for electromagnetic continua, Math. Mech. Solids 14 (4) (2009) 390–402. http://dx.doi.org/10.1177/1081286507080808.
[21] J.D. Jackson, Classical electrodynamics, Classical Electrodynamics, third ed., Wiley-VCH, 1998, pp. 832. ISBN 0-471-30932-X.
[22] H. Montgomery, Current flow patterns in a faraday disc, Eur. J. Phys. 25 (2) (2004) 171.
[23] M. Rubin, Cosserat theories: shells, rods and points, in: Solid Mechanics and its Applications, vol. 79, Kluwer Academic Publishers, Dordrecht, 2000.
[24] A. Queiruga, A computational model of electromagnetically sensitive fabric armor colliding with a rigid projectile (Master's thesis), University of California, Berkeley, 2013.
[25] M. Griebel, T. Dornseifer, T. Neunhoeffer, Numerical Simulation in Fluid Dynamics: A Practical Introduction, Vol. 3, Siam, 1997.
[26] T. Zohdi, High-speed impact of electromagnetically sensitive fabric and induced projectile spin, Comput. Mech. 46 (3) (2010) 399–415.
[27] T. Zohdi, Electromagnetically-induced deformation of functionalized fabric, J. Elasticity 105 (1) (2011) 381–398.
[28] R.J. LeVeque, Finite Difference Methods for Ordinary and Partial Differential Equations: Steady-State and Time-Dependent Problems, Vol. 98, Siam, 2007.
[29] R. Alexander, Diagonally implicit runge-kutta methods for stiff ode's, SIAM J. Numer. Anal. 14 (6) (1977) 1006–1021.
[30] S. Van Der Walt, S.C. Colbert, G. Varoquaux, The numpy array: a structure for efficient numerical computation, Comput. Sci. Eng. 13 (2) (2011) 22–30.
[31] E. Jones, T. Oliphant, P. Peterson, et al., SciPy: Open source scientific tools for Python, [Online; accessed 2016-01-01] (2001–). URL http://www.scipy.org/.
[32] Wolfram Research, Inc., Mathematica, version 9.0 Edition, Wolfram Research, Inc., Champaign, Illinois, 2012.
[33] J.D. Hunter, Matplotlib: A 2d graphics environment, Comput. Sci. Eng. 9 (3) (2007) 90–95.
[34] A. Henderson, J. Ahrens, C. Law, et al., The ParaView Guide, Kitware Clifton Park, NY, 2004.
[35] J.C. Butcher, The Numerical Analysis of Ordinary Differential Equations: Runge–Kutta and General Linear Methods, Wiley-Interscience, 1987.
[36] M. Crouzeix, Sur l'approximation des équations différentielles opérationnelles linéaires par des méthodes de runge-kutta (Ph.D. thesis), 1975.
[37] S.P. Norsett, Semi explicit Runge–Kutta methods, Matematisk Institut, Universitet I, 1974.